24

25

33

29

Coline Ariagno^{1,2}, Philippe Steer¹, Pierre G. Valla², Benjamin Campforts³

⁴Université ¹Univ.Rennes, CNRS, Géosciences Rennes UMR 6118, 35000 Rennes, France ²ISTerre, Grenoble CNRS

²Univ. Grenoble Alpes, Univ. Savoie Mont Blanc, CNRS, IRD, Univ. Gustave Eiffel, ISTerre Institut des Sciences de la Terre, 38000 Grenoble, France

³ Department of Earth Sciences, VU University Amsterdam, Netherlands

Correspondence to: Coline Ariagno (coline.ariagno@univeuniv-rennes.fr)

Abstract. In steep alpine environments, successive glacial-interglacial cycles during the Quaternary led to multiple transient geomorphological phases. In particular, post-glacial periods are key transition phases experiencing rapid geomorphic changes, characterized by intense hillslope processes where ice and permafrost have retreated. Mass wasting is the dominant post-glacial process driving sediment production in steep mountain landscapes. However, its role in shaping topography, particularly in comparison to glacial activity—known for its strong deformational impact—remains poorly understood. By integrating numerical modeling with topographic data, we refine our understanding of how mass wasting shapes an evolving landscape and influences sediment dynamics. In the Ecrins massif (French western Alps), we select three catchments, with particular morphological signatures or inheritance (i.e. from fluvial to glacial), to model their associated topographic evolution driven by mass wasting. Using the landscape evolution model 'HyLands', we quantitatively assess their individual response to landsliding by exploring the role of different internal or external factors (e.g., bedrock cohesion and friction, return time of landslides). The model is calibrated with the output landslide areavolumefrequency scaling law and the massif-averaged denudation rate, inferred from literature. We focus on the cumulative impact of landslides, over a single post-glacial period, on catchment slope distribution, hypsometry, produced exported sediment volume and erosion rate. Compared to a fluvial ones, landscape, the inherited glacial topography shows a bimodal distribution of elevation for unstable slopes, near the crests and along the U-shapeshaped valley walls. The time evolution of this distribution is characterized by a decrease in the number of unstable slopes as well as a lowering in maximum catchment elevations induced by landsliding, usually attributed to the glacial buzzsaw. Indeed, glaciers may be not the only agent controlling mountain elevation, as we discussed in this study. Despite the stochastic nature of landslides, our modeling results also show that landslide activity and induced erosion rates are maximumgreatest at the onset of the glacial retreat and then progressive progressively decay during the interglacial period. On the contraryIn contrast, fluvial catchments show a more stable topography and less intense landslide activityfewer landslides resulting in lower erosion rates. This study quantitatively explores the non-linear interactions between landslides and catchment topographic Style Definition: Bibliography: Indent: Left: 0 cm, First

line: 0 cm, Space After: 12 pt, Line spacing: single

evolution and questionsdocuments the role of landslides in the erosion pulse during the Quaternary interglacial periods.

42 43

44

45

46

47

48

49 50

51

52

53 54

55

56

57

58

59

60

61

62

63 64

65

66 67

68

69 70

71

72

73

74

75 76

41

1. Introduction

The Quaternary period is characterized by oscillations from glacial to interglacial cycles overprinting a global climatic cooling trend over the Cenozoic era (Zachos et al., 2001). These successive climatic transitions have been suggested to be associated with abrupt and transient geomorphologic and topographic changes (Champagnae et al., 2014; Peizhen et al., 2001). (Champagnae et al., 2014; Peizhen et al., 2001; Zhang et al., 2022). In high-latitude regions and mountain ranges, glaciers are usually considered as the main geomorphic and erosion agents (Hallet et al., 1996; Herman et al., 2013, 2021; Herman & Champagnac, 2016; Métivier et al., 1999).(Hallet et al., 1996; Herman et al., 2013, 2021; Herman and Champagnac, 2016; Métivier et al., 1999). The topographic changes resulting from glacial erosion are progressive and spatially variable over a single or multiple glacial-interglacial cycle (Seguinot & Delaney, 2021)(Seguinot and Delaney, 2021) of the Quaternary (Herman et al., 2011; Pedersen & Egholm, 2013; Sternai et al., 2013; Tomkin & Braun, 2002). (Herman et al., 2011; Pedersen and Egholm, 2013; Sternai et al., 2013; Tomkin and Braun, 2002). Glaciated landscapes have in turn been widely studied to better understand past glacier dynamics and quantify glacial erosion rates and associated topographic changes at the Earth's surface (Ganti et al., 2016; M. Koppes et al., 2015; Pedersen & Egholm, 2013; Peizhen et al., 2001; Solomina et al., 2015; Sternai et al., 2013).(Ganti et al., 2016; Koppes et al., 2015; Pedersen & Egholm, 2013; Peizhen et al., 2001; Solomina et al., 2015; Sternai et al., 2013). Glacial and periglacial processes have strongly imprinted mountainous landforms, shaping U-shaped valleys, but also cirques, arêtes and hanging valleys, all characterized by marginal steep slopes and rugged topography (e.g. Anderson et al., 2006; Penck, 1905; Prasicek et al., 2015). In turn, glacial morphological features likely represent transient and mechanically unstable landforms under interglacial conditions (Herman & Braun, 2008; Prasicek et al., 2015)(Herman and Braun, 2008; Prasicek et al., 2015), dominated by hillslope and fluvial processes. Understanding the interglacial evolution of formerly glaciated landscapes has remained challenging since it involves complex non-linear geomorphic processes and interrelated spatial/temporal scales. Yet, this is a major need for assessing the ongoing response of mountainous environments to current climate warming (e.g. Zhang et al., 2022). Interglacial periods are associated with overall warming climatic conditions, leading to a progressive cryosphere degradation (i.e. glacier retreat and permafrost recession), and in turn to a shift of the main geomorphic and erosion processes. Under interglacial conditions, paraglacial (Ballantyne, 2002) and periglacial (French, 2017) processes become more efficient and affect larger mountainous areas. Hillslope processes, including landsliding, rockfall and soil creep, affect formerly glaciated mountain slopes. Rivers transport remobilized and newly-produced sediments (Roussel et al., 2018) and can locally re-incise glacial valleys (e.g., Leith et al., 2018; Valla et al., 2010). Over the Quaternary,

Formatted: Outline numbered + Level: 1 + Numbering Style: 1, 2, 3, ... + Start at: 1 + Alignment: Right + Aligned at: 0.5 cm + Indent at: 1.13 cm

Quaternary could have led to an increase in erosion, and sediment flux (M. Koppes et al., 2015; M. N. 80 81 Koppes & Montgomery, 2009; Peizhen et al., 2001)(Koppes et al., 2015; Koppes & Montgomery, 2009; Peizhen et al., 2001) and topographic relief (Champagnac et al., 2014), rather than the supposed greater 82 83 efficiency of glacial erosion itself (Koppes and Montgomery, 2009). 84 In the following work, we focus on the transient phase from glacial to interglacial conditions, hereinafter 85 referred to as the post-glacial period, i.e. when alpine glaciers retreated and left uncovered 86 landscapel and scapes dominated by non-glacial geomorphic agentsprocesses. In this context, steep parts 87 of mountain hillslopes becomebecame more prone to mass wasting processes, favored by glacial 88 debuttressing (E. Cossart et al., 2008)(Cossart et al., 2008) and permafrost retreat (e.g. Cathala et al., 2024; Lebrouc et al., 2013). The rapid climate change observed over the last decades has motivated 89 90 research on the evolution of permafrost and its impact on high-elevation rockwall dynamics (Gallach et 91 al., 2020; Magnin et al., 2017; Ravanel et al., 2017; Stoffel et al., 2024). In addition, gravitational instabilities, such as bedrock landslides or rockfalls, are widespread in mountainous landscapes and 92 93 appear as one of the most efficient processes to shape them (Keefer, 1984). Taking over glacial erosion, 94 hillslope Hillslope activity transiently reshapes glacial morphological features leading to a postglacial 95 increase in both the frequency and intensity (related to the volume) of hillslopemass wasting events through time (e.g. Korup, 2006; Zerathe et al., 2014). Landslides significantly contribute to catchment-96 97 scale erosion by mobilizing large bedrock volumes, which greatly impact sediment fluxes (Broeckx et 98 al., 2020; Hovius et al., 1997; Zech et al., 2009). As a positive feedback loop, by decreasing the local baselevel, fluvial sediment export and local incision of formerly glaciated valleys; can foster the 99 100 hillslope response. The postglacial period is also associated towith major changes in the hillslope-101 channel connectivity (Brardinoni & Hassan, 2007; Cavalli et al., 2019; Müller et al., 2022)(Brardinoni 102 and Hassan, 2007; Cavalli et al., 2019; Müller et al., 2022), and in the drainage system (Comiti et al., 103 2019; Lane et al., 2017; Pitlick et al., 2021; Zhang et al., 2022). As such, this period appears complex 104 due to rapid morphological changes and multiple geomorphic processes that all interact and drive major 105 changes in both the hillslope domain and the drainage network. However, while previously-cited studies 106 have already explored the geomorphological role of landslides during the last interglacial period, 107 understanding which landscape areas are more affected during the postglacial times and how this 108 landslide activity is distributed through both space and time remains mainly unanswered and not

quantified. Therefore, quantifying the spatio-temporal impact of landslides on evolving postglacial

landscapes is needed to better understand sediment production, transfer and potential storage along the

source to sink pathway and assess the overall topographic evolution in mountainous environments.

repetitive climatic oscillations between glacial and interglacial periods have caused frequent mismatches

between dominant geomorphological processes and the organization or shape of the landscape on which

they act. This has led to the hypothesis that these transient climatic/geomorphic conditions over the

77

78

79

109

110

111

Formatted: English (United States)

Field Code Changed

HWhile the landsliding impact on mountain topography appears clear after a single triggering event, such as a storm or an earthquake (Dahlquist et al., 2018; Meunier et al., 2008; Morriss et al., 2023; J. Roering, 2012), their role in long term shaping of mountain range is not straightforward. For investigating(Dahlquist et al., 2018; Meunier et al., 2008; Morriss et al., 2023; Roering, 2012), their role in long-term shaping of mountain ranges is not straightforward. To investigate the post-glacial period, landslide catalogues (Blondeau et al., 2021; Wood et al., 2015), bedload records (Lane et al., 2017), remote-sensing and geophysical methods have intrinsic limitations and integration times that are too short. Conversely, long-term mountain erosion estimates from geochronological and thermochronological methods (Herman et al., 2013) or large-scale sediment budgets (Kuhlemann et al., 2002) may have too long integration times to investigate interglacial periods. Terrestrial cosmogenic nuclides (TCN) have been commonly used to quantify catchment-wide erosion rates over 10² - 10⁵ yr timescales (Brown et al., 1995; Delunel et al., 2020; Mudd et al., 2016; Portenga & Bierman, 2011) These approaches also cannot be generally used to disentangle the impacts of individual processes like landsliding from other forms of erosion. Terrestrial cosmogenic nuclides (TCN) have been commonly used to quantify catchment-wide erosion rates over $10^2 - 10^5$ yr timescales (Brown et al., 1995; Delunel et al., 2020; Mudd et al., 2016; Portenga and Bierman, 2011), covering glacial-interglacial cycles. Although this approach appears meaningful to address the postglacial period (~10-20 kyr), TCN-derived erosion rates are punctual and averaged in both space (catchment) and time. In turn, this prevents exploring in detail the spatial distribution and temporal evolution of erosion during that period, as well as discriminating the different active geomorphological processes. Moreover, the cosmic ray attenuation depth, (~60 cm), which sets the integration time of TCN (von Blanckenburg, 2005), can be significantly smaller than the depth of large to gigantie (von Blanckenburg, 2005), can be significantly smaller than the depth of large landslides observed in formerly glaciated catchments (Korup, 2006; Lavé et al., 2023).(Korup, 2006; Lavé et al., 2023; Niemi et al., 2005). Overall, this raises the question of the potential limitations of TCN-derived erosion rates in constraining the time evolution of post-glacial erosion in landscapes dominated by bedrock landsliding. In this context, landscape evolution modelling (LEM) appears as a relevant approach to overcome the limited amount of data/observations and the intertwined spatial and temporal scales involved (Tucker & Hancock, 2010).(Tucker and Hancock, 2010). Numerical modelling can combine complex surface processes, including tectonic uplift, hillslope and river dynamics integrating all the sediment transfer cascade and hillslope-channel connectivity, while allowing predictions of topographic evolution or sediment production rates c over large spatial and temporal scales. Different categories of models can be considered to study mass wasting processes (Campforts et al., 2022). Physical-based models produce

realistic debris flow (and river) propagation and deposition but may not be adapted for large scale

landscape evolution (Croissant et al., 2017; Davy et al., 2017; Dietrich et al., 1995; George & Iverson, 2014; Hergarten & Robl, 2015; Martin et al., 2023). Landscape evolution models (LEM) rather use

112

113

114

115

116

117

118

119120

121

122

123

124

125

126

127

128

129

130

131

132

133

134

135

136

137138

139

140

141

142

143

144

145

146

147

Formatted: French (France)

reduced complexity geomorphic laws to simulate the evolution topography over possibly long timescales and large spatial scales (Carriere et al., 2020; Langston & Tucker, 2018; Liebl et al., 2021). For instance, linear or non-linear diffusion laws are generally used to simulate hillslope erosion in most LEMs (Heimsath et al., 2005; Perron, 2011; J. J. Roering et al., 1999). Soil-covered models simulate shallow landslides to follow for instance the impact of rainfall variability at large scale (Claessens et al., 2007), while bedrock landslide models allow the distinction between constant and episodic sediment production through landslides (Campforts et al., 2020; Densmore et al., 1998). Therefore, numerical modelling offers multiple ways to simulate hillslopes processes, and their interactions, by highlighting diverse approaches, modeling complexity and spatio-temporal scales.

. Physically-based models produce realistic debris-flow (and river) propagation and deposition but may not be adapted for large-scale landscape evolution (Croissant et al., 2017; Davy et al., 2017; Dietrich et al., 1995; George and Iverson, 2014; Hergarten and Robl, 2015; Martin et al., 2023). Landscape evolution models (LEM) instead use reduced-complexity geomorphic laws to simulate the evolution of topography over possibly long timescales and large spatial scales (Carriere et al., 2020; Langston and Tucker, 2018; Liebl et al., 2021). Therefore, numerical modelling offers multiple ways to simulate hillslope processes, and their interactions, by highlighting diverse approaches, modeling complexity and spatio-temporal scales.

The aim of this study is to explore numerically, using a stochastic and reduced-complexity model, the role of landslides in the postglacial morphological dynamics of mountainous landscapes. We use the HyLands model (Campforts et al., 2020, 2022), which explicitly simulates bedrock landslides, to predict associated mass redistribution and the resulting catchment-averaged erosion rates and topographic evolution through multiple timescales. We investigated investigate the topographic impact of landslide activity on selected Alpine catchments, located in the Ecrins massif (France), showcasing a gradient of glacial imprint and deglaciation timing. An open question is the role of interglacial processes in erasing the inherited morphological signature of former glaciation, leading to an erosional "hotmoment". More specifically, we aim to assess the timescales, rates and locations of topographic changes associated with the transient shift from glacial to interglacial periods, with a particular focus on the role of landsliding. Our main working hypothesis is that the different morphological signatures observed for Alpine catchments are evidencing both landslide activity and deglaciation timing. Alpine catchments do show a glacial topographic imprint, and here we test the capacity of landslides to (at least partly) reshape this glacial topographic inheritance over the postglacial period. The first objective of the study is to conduct a spatial analysis of simulated landslides to assess their magnitudes and locations within the investigated catchments. Then, a temporal analysis is performed to investigate whetherthe duration of the postglacial period remains a transient phase and, in other words, how long it may require to achieve an interglacial steady-state topography (i.e., referring to the end of the transient phase), and erosion dynamics under landslide activity.

186

187

188 |189

190

191

192

193

194

195 |196

197

198

199

200

201

202

203

204

205

206

207

208

209

210

211

212

213

214 215

216

217

218 219

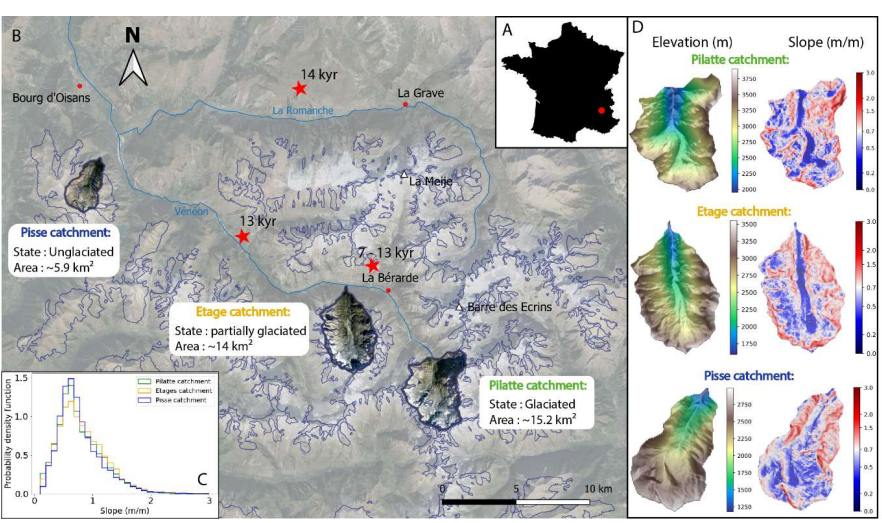
2. Study area

2.1 Tree selected Selected catchments in the Ecrins massif

The Ecrins massif (south-east France, Fig. 1A) forms a high-elevation high-relief area of the southwestern Alps, and today still hosts glaciers in its upper catchments. The present-day topography was deeply impacted by glaciation (van der Beek & Bourbon, 2008), and several studies have focused on constraining the timing and extent of the Last Glacial Maximum (LGM, ca. (van der Beek and Bourbon, 2008), and several studies have focused on constraining the timing and extent of the Last Glacial Maximum (LGM, ca. 20 ka) and post-LGM glacier fluctuations (Delunel et al., 2010; Le Roy et al., 2017). In this context, we select three small (6 – 15 km² area) catchments to cover the entire Vénéon valley, from the river source, at the heart of the Ecrins massif, to the confluence with the Romanche river where tributary glaciers had a lower morphological impact (Fig. 1B). The Pilatte catchment, the highest and most glaciated catchment, peaks at ~3600 m above sea level (a.s.l.), with valley bottoms around and has a minimum elevation of 2000 m. Modern glaciers represent ~14% of the eatehment area (total catchment area of approximately 15 km²); With a downstream direction toward the north, its western and eastern parts are made of granitic orand migmatic rocks (gneiss), respectively (source: French Geological Survey BRGM)-, https://infoterre.brgm.fr/). The Etages catchment, partiallyglaciated at present-day (~12 %), displays similar characteristics with an area of ~14 km² and an elevation range from 3564 to 1600 m a.s.l. at the confluence with the Vénéon river. The catchment is mainly underlaid by granites with crestlines composed of gneiss in its south-eastern part (Barféty et al., 1984; Delunel et al., 2014). Both catchments show steep hillslopes (>45-60(up to ~2.2 m/m, i.e., 65°, Fig. 1C), located on the walls of the main U-shaped valley and along the highest rockwalls, considered as nunataks (Delunel et al., 2010; Marx et al., 2017), and a low-relief central valley bottom (Fig. 1D). The Etages catchment has been investigated by Delunel et al., 2014, with a detailed geomorphological mapping and the use of quartz ¹⁰Be concentrations in detrital material to trace the potential geomorphic sources for river sediments. The thirdFinally, the Pisse catchment, called "La Pisse", is completely unglaciated today and is smaller than the two other catchments (~6 km² total area). Its highest elevation at ~3050 m occurs at its southern crest, while its lowest elevation of ~1250 m is at the confluence with the adjacent Villard catchment. Its lithology is dominated by granites even if thewith some Jurassic limestones along its southwestern crest-shows few Jurassic limestone outcrops. Slopes are mostly gentle in the upper part of the catchment and get steeper downstream along the valley rockwalls. Despite different glacial imprints and elevation, the slope distributiondistributions for the studied catchments isare relatively similar (Fig. 1C), with a modal slope around 35° (0.7 m/m) for all three catchments.

These <u>3three</u> investigated catchments have experienced a gradual post-LGM deglaciation, following the progressive glacier retreat along the Vénéon valley from downstream (Pisse catchment) to upstream

Formatted: Outline numbered + Level: 1 + Numbering Style: 1, 2, 3, ... + Start at: 1 + Alignment: Right + Aligned at: 0.5 cm + Indent at: 1,13 cm (Pilatte catchment). Following Delunel (2010), the Pisse catchment has likely started its deglaciation around 15 ka, (based on deglaciation constraints upstream and downstream in the Romanche valley, e.g. Schwartz et al., 2017), while the EtageEtages catchment may have been deglaciated between 13 and 7 ka. (Fig.1B). The glacier retreat in the Pilatte catchment has probably started slightly after the EtageEtages catchment and can be considered at the end of the post-LGM deglaciation. As a consequence, the observed delay in glacier retreat between the three catchments (Fig. 1A) has likely been associated with a time-transgressive activation of periglacial processes like landslides, resulting in different topographic configurations today.



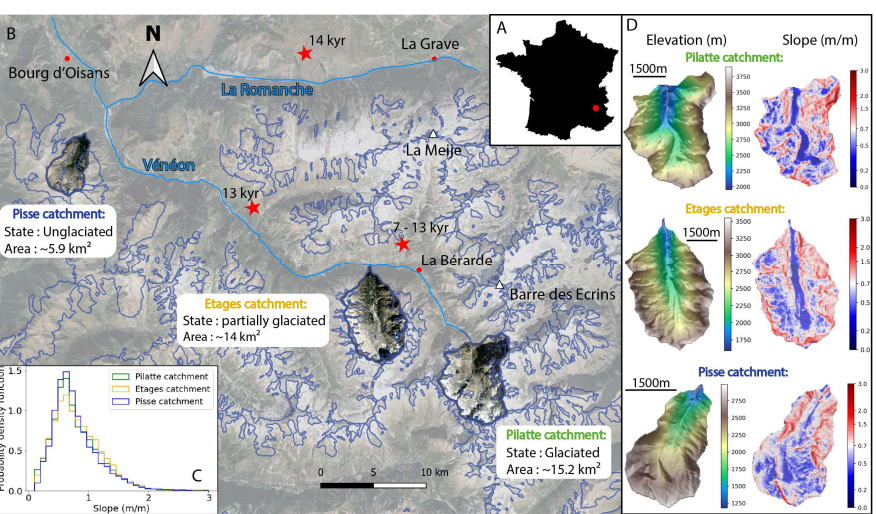


Figure 1: Geomorphological context of the study area. A) Location of the Ecrins massif (red dot) in France. B) Google satellite image of the Ecrins massif (background) with the three studied catchments and their characteristics: Pilatte (green label), Etages (yellow label) and Pisse (blue label). Blue thin line indicates the contour of the LGM ice extent (Delunel, 2010). Red stars report the estimated deglaciation timing (exposure of glacially-polished bedrocks and erratics; Delunel, 2010). C) Probability density function of topographic slope for the three studied catchments (25-m resolution DEM from the French National Geographic Institute IGN). Similar distributions are observed, with a main slope mode around 0.7 m/m. D) Modern elevation and slope maps for the three studied catchments.

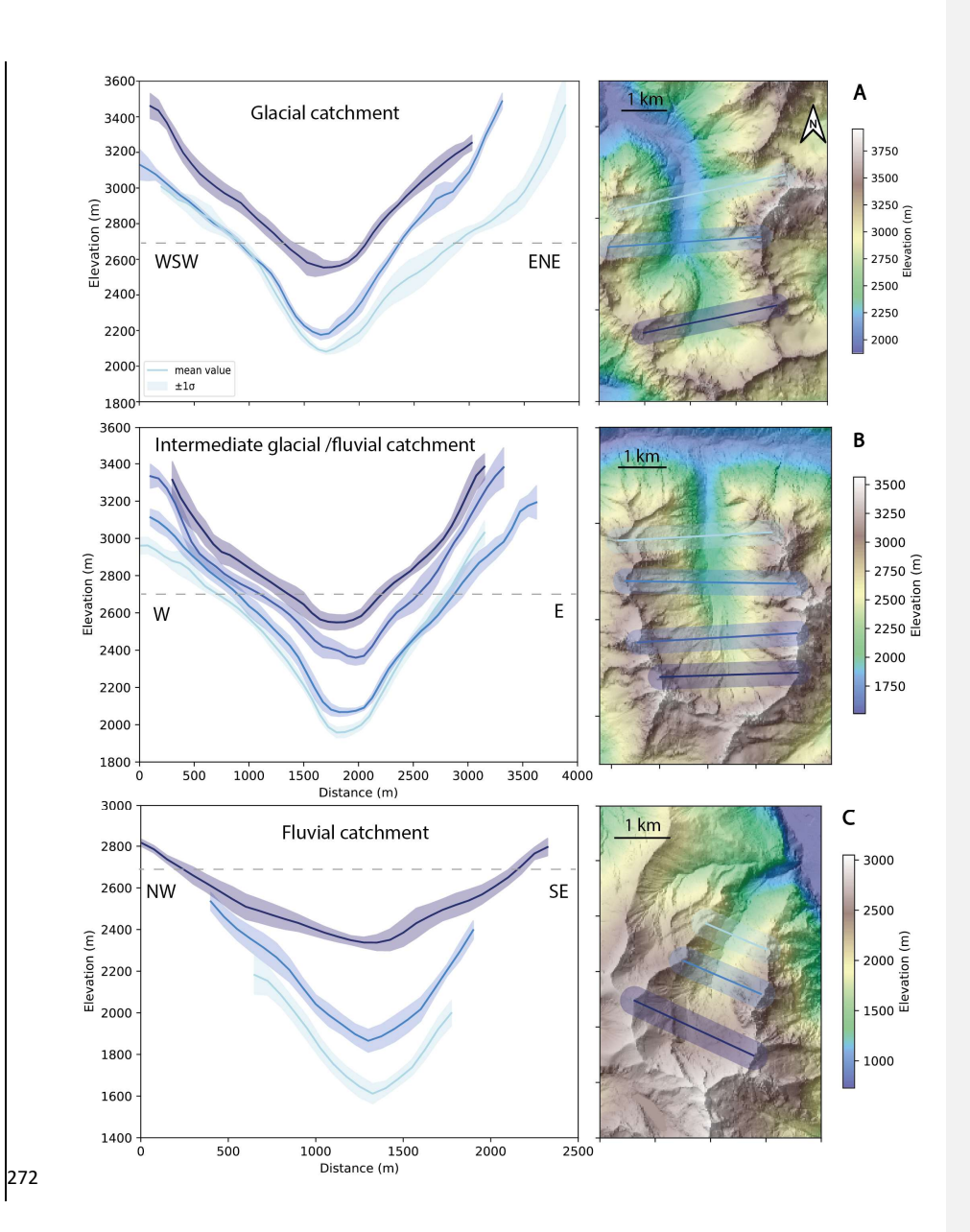
2.2 Characteristics of glacial-catchment 2.2 Catchment hillslope profiles

To visualize the hillslope morphologies in our studied catchments, we made topographic transects (Fig.2) along the main valley. In the literature or on the field, classical perpendicular to the trunk stream in each catchment. Classical glacial topographic features, including typical U-shape valleys (Fig. 3), are

well documented, easily observable and have been suggested to result from the bimodal distribution of glacial erosion with elevation (e.g. Anderson et al., 2006; Egholm et al., 2009; Herman et al., 2011; Steer et al., 2012). (Anderson et al., 2006; Bernard et al., 2025; Egholm et al., 2009; Herman et al., 2011; Steer et al., 2012). The observed bimodal hypsometry of glacial landscapes (Brocklehurst & Whipple, 2006) (Brocklehurst and Whipple, 2006) defines the boundaries between the valley overdeepening, driven by fast-moving ice with intense erosion by abrasion and quarrying, and areas with slower-moving ice exerting less erosive power (Coutterand, 2010; Leith et al., 2014). Alternatively, this bimodal hypsometry may be attributed to different patterns of cold-climate erosion around the ELA (Equilibrium Line Altitude) (Liebl et al., 2021). In both interpretations, the hillslope shoulder – a slope inflection between two steep upper and steep lower hillslopes, known as "shouldering" (Fig. 2 – conceptual figure), - is shaped during glacial periods (Louis, 1952; Valla, 2021). This topographic shouldering would result in a bimodal distribution of catchment elevations with steep slopes associated to both the glacier valley flanks (low elevations) and to the nunataks-crestlines area (i.e. periglacial regions at high elevations) (Coutterand, 2010; Liebl et al., 2021).

In our studied eatchments, the Our two upper catchments (Pilatte and Etages catchments) highlight theshow a clear U-shaped valley on each transect, even in the upstream part of the catchment. A slope inflexioninflection is also visible along most of the transects, which we refer to interpret as "evidence of shouldering" (Fig. 3). For most of the transects, the increase in slope furthest upstreamupslope of the shouldering corresponds to the glacial trimline (Penck, 1905). It corresponds to the highest zone of the glacier extent and usually the limit between prevailing glacier erosion processes and periglacial processes, as their elevations whose locations match with the upper limits of the glacier cirque (Rootes & Clark, 2020)(Rootes and Clark, 2020) (Fig. 2). Conversely, the topographic transects for the unglaciated catchment (Pisse) tend to reveal a V+ shape-shaped valley, especially in the lower part of the catchment. The upper profile, however, is closer to those of the glacial and intermediate eatchments, showing a clear inheritance from previous glaciations.

In the following, we will name the three studied catchments according to their glacial morphology imprint, i.e 'glacial', 'intermediate glacial-fluvial' and 'fluvial' for the Pilatte, Etages and Pisse catchments, respectively.



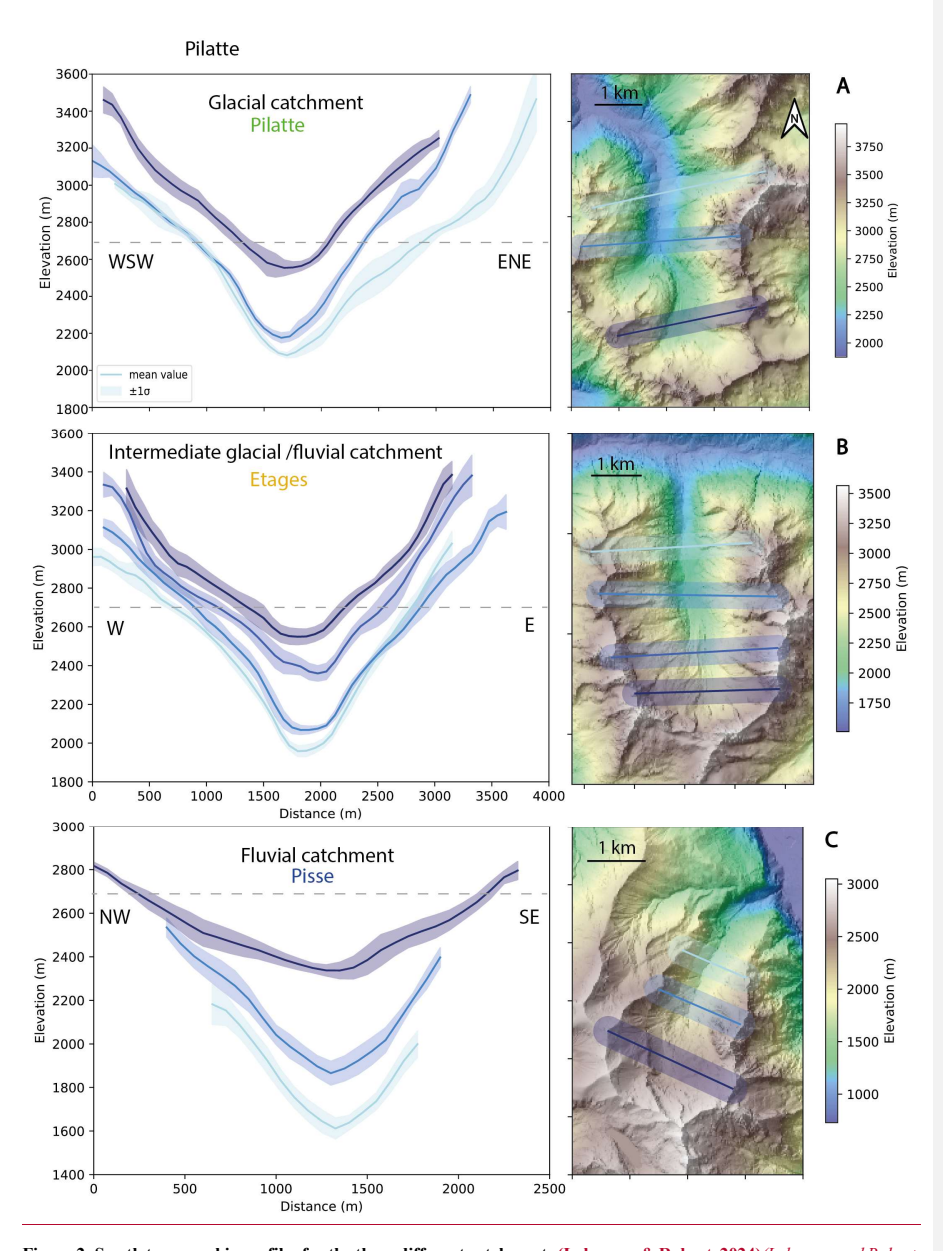


Figure 2: Swath topographic profiles for the three different catchments (Lehmann & Robert, 2024)(Lehmann and Robert, 2024) (DEM, resolution: 50 cm, ESPG2154, from the French National Geographic Institute, Cusicanqui, 2024Cusicanqui, 2024): (A) Glaciated catchment (Pilatte), (B) intermediate glacial-fluvial catchment (Etages), and (C) fluvial catchment (Pisse). Profiles are aligned based on their lowest area. The grey dotdashed line illustrates the 2700 m elevation, a threshold elevation where around which the predicted landslides activity is lower (Figs. 6 & 7).

3. Modeling framework

280

. 281

282

283

284

285

286 287

. 288

289

290

291

292

293

294

295 296 297

|298 |299 |300 |301 Hylands is a reduced-complexity and stochastic landslide model (Campforts et al., 2020, 2022). It simulates both the erosion associated with deep-seated-gravitational landslides and the induced sediment transport and deposition resulting from landslide runout. Hylands is part of the Landlab open-source framework (Barnhart et al., 2020; Hobley et al., 2017), which offers tools to combine multiple geomorphic laws on 2D regular grids, potentially applied to either synthetic topographies or digital elevation models (DEMs). In the following, we use the 25-m resolution DEMs from the IGN (BD ALTI of IGN (, French National Geographic Institut), Institute, https://www.ign.fr/), as initial model topographies for the three studied catchments. The catchment boundaries were obtained from the geo-"Eau France" website: tools ("available the service processing at https://reseau.eaufrance.fr/geotraitements/viewer/bassin-versant)--. We first here present the model and then our strategy for model calibration.

Fluvial landscape

Landslides area

Glacial landscape

Nunatak

Trimline zone

Shouldering

Valley
U-shaped
flanks

A

B

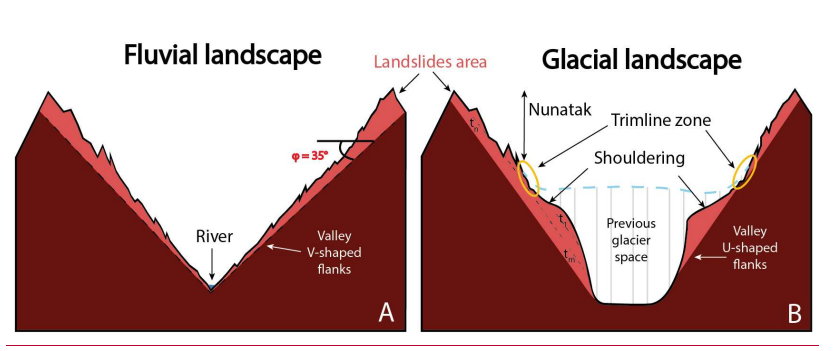


Figure 3: Conceptual sketches of theoretical topographic-fluvial (A) and glacial (CB) landscapes. A) Typical landscape dominated by fluvial erosion processes with V-shaped valley and homogeneous hillslopes slightly above the internal angle of friction ($\phi=35^\circ$ in this example). B) Landscape dominated by glacial erosion processes. The main morphological characteristics such as U-shaped valley, periglacial nunatak zone, shouldering orand the trimline zone (yellow circle) are shown (modified from Louis, 1952; Coutterand, 2010). The light-red color indicates potential landscape areas affected by landslide activity: where different failure planes, associated to particular times, are illustrated (dashed black line and t_i , t_m , t_m).

Formatted: Outline numbered + Level: 1 + Numbering Style: 1, 2, 3, ... + Start at: 1 + Alignment: Right + Aligned at: 0,5 cm + Indent at: 1,13 cm

3.1 The HyLands model

3.1.1 Landslide triggering

In HyLands, the landslide source model combines a spatial probability P_s and a temporal probability P_t to compute a landslide failure probability $P_{failure} = P_s * P_t$. The spatial probability is computed following a modified Culmann criterion (Campforts et al., 2020; Culmann, 1875), which is a Mohr-Coulomb criterion applied to a finite slope analysis:

$$P_{s} = \frac{H_{s}}{H_{c}},$$
 with $H_{c} = \frac{4C}{\rho g} \frac{\sin \beta \cos \varphi}{1 - \cos(\beta - \varphi)},$ (1)

where H_s (m) is the local hillslope height calculated between two adjacent cells of the grid and H_c is the maximum stable hillslope height (m), which depends on the cohesion C (kg.m⁻¹.s⁻²), ρ the rock density set to 2700 kg.m⁻³, g = 9.81 m.s⁻² the gravitational acceleration, β the local topographic angle, and φ the angle of internal friction (Eq. 1). Both C and φ are parameters that need to be calibrated in our modelling approach.

However, HyLands is not a deterministic model as it combines this spatial probability of failure to a temporal probability. Indeed, P_t controls the temporal occurrence of landslides and follows a Poisson law (Campforts et al., 2022):

319
$$P_t = 1 - e^{-\frac{t}{t}}/t_{LS}, \tag{2}$$

where t (dt = 10 yr) is the simulation time step which remains constant during the model time and runs. t_{LS} (yr) is the return time of landslides triggering events. In turn, if any slope change occurs, the probability of failure $P_{failure}$ of a given cell increases is constant with time, until $P_{failure}$ becomes greater or equal to one, leading to landslide triggering, and is updated at very model iteration. The simulation time step is set to dt = 10 yr random nature of landslides is introduced using a grid of cells with a random number r between 0 and 1. Landslides will occur if $r \ge P_{failure}$ at a particular cell (Campforts, Shobe et al, 2020). Generating a different grid of r value, by setting the seed parameter differently, will necessarily induce a different pattern of landsliding.

3.1.2 Landslide erosion and deposition

When a landslide event is triggered, the erosion scar generates a failure plan whichplane initiates at the triggering point, generating an erosion scar. Following the Culmann criterion, the dip angle of this plan θ_{τ} is the bisector of the local topography angle β , and the angle of internal friction of the material φ :

$$\theta = \frac{\beta + \varphi}{2} \tag{3}$$

The failure plane is propagated upstream of the critical node if the elevation of the neighboring cells exceeds the rupture surface. In this case, all the DEM cells above this surface are considered as unstable and mobilized by landsliding.

Landslide-derived sediments can either be transported as wash load, determined by the fraction of fines, Ff in the model, or redistributed using a non-local nonlinear deposition scheme (Campforts et al., 2022). Because our first goal is to study landslide erosion without any potential feedback of deposited sediments, we set the fraction of fine sediments Ff to 1, meaning that all sediments are instantaneously evacuated. Because our primary goal is to study landslide erosion without any potential feedback of deposited sediments, all sediments are instantaneously evacuated in this setup. It also means that in our set-up no topographic change can occur below the triggering points of simulated landslide sources.

3.2 Strategy for model calibration

Our objective is to use a calibrated and physically sound landscape evolution model, based on HyLands, to predict landslide activity during postglacial conditions in our study area. Note that in these simulations, we only consider the role of landslides in landscape evolution and erosion dynamics, without modeling fluvial erosion nor tectonic activity (e.g., uplift rate). We also assume that gravitationally triggered landslides as simulated in HyLands, represent the combination of mass wasting events in alpine topography including rockfalls, debris flows, and shallow to deep-seated landslides, capturing the diverse range of slope failure processes. Our model calibration is performed on the Etages catchment following two steps:

- 1) Calibrating φ and C, which control the spatial probability of landslide occurrence, by comparing the modelled landslides area-frequency distribution (3.3.2) and size-volume scaling relationship (3.3.3), with the ones of those taken from natural landslide datasets elsewhere (Fig. 4; Delgado et al., 2022; Guzzetti et al., 2002).
- 2) Calibrating the landslide return time t_{LS} , which sets the temporal probability of landslide occurrence, by comparing modelled catchment-averaged erosion rates and observed erosion <u>rates</u> data derived from quartz ¹⁰Be concentrations in stream sediments (3.3.4, Fig. 5), ranging between 0.27 and 1.1 mm/yr in the Ecrins massif (Delunel et al., 2010). For the Vénéon valley and the studied catchments (i.e. Etages catchment), we can reduce <u>the interval fromthis range to</u> 0.7 to 1.1 mm/yr for our model calibration (Fig. 5). Assuming that a rock sample records quartz ¹⁰Be accumulation over the time period corresponding to <u>removal of</u> the upper 60 cm <u>below the surfaceof rock</u> (Delunel et al., 2010; von Blanckenburg, 2005), <u>these</u> ¹⁰Be-derived erosion rates record apparent integration times of around 500 to 2500 yr. We thus select a simulation time of 1500 yr for the model calibration phase.

Some combinations of parameters (φ, C, t_{LS}) lead to too few landslides, preventing a statistical analysis of their resulting size distribution. To overcome this issue, we generatedgenerate a large amount of landslide events and selected a similar number of landslides per simulation. ThenTo do this, we hadneed

to(1) compile multiple simulations with similar parameters but different stochastic occurrence (different seeds), (2)) and reduce the return time (from $t_{LS} = 1 \times 10^5$ yr to $t_{LS} = 100$ yr). Because t_{LS} controls the occurrence of landslides without impacting their geometry, a small value of t_{LS} induces simulation outputs with large landslide datasets. This is particularly true given that the potential for landsliding remainremains significant throughout the simulation. The first approach wasis used for all the parameter calibration (Figs. 4A-C, 5), while the second approach was only used in the landslide size-frequency calibration (Fig. 4A) because the modified return time value can induce changes in landslide volumes and occurrences, and thus in output catchment-averaged erosion rates (Fig. 5).

.

.

3.3 Model calibration

3.3.1 Calibration of the angle of internal friction: landslide area-frequency distribution

Because we are lacking detailed compilation of alpine mass-wasting events, HyLAndsHyLands will be calibrated against global compilations of landslide data. More specifically, we aim at constraining the cohesion and angle of internal friction parameters. Although not calibrated to our specific to our field site, this general calibration will allow assessing the impact of gravity driven erosion in high alpine terrain and therefore providesproved sufficient for this study. For our calibration runs, we run HyLands from existing topography of the three catchments and set model parameters not involved in the calibration equal to those as reported in Table S1.

Field inventories of landslides and rockfalls show a well-known shape for the frequency distribution of landslide area, highlighting several characteristics of a power-law relationship (Delgado et al., 2022; Guzzetti et al., 2002; Jeandet et al., 2019; Malamud et al., 2004; Stark & Hovius, 2001; Tanyaş et al., 2019; Tebbens, 2020)(Delgado et al., 2022; Guzzetti et al., 2002; Coulomb Mechanics and Relief Constraints Explain Landslide Size Distribution - Jeandet - 2019 - Geophysical Research Letters - Wiley Online Library, 2023; Landslide Scaling: A Review - Tebbens - 2020 - Earth and Space Science - Wiley Online Library, 2023; Malamud et al., 2004; Stark and Hovius, 2001; Tanyaş et al., 2019): (1) the rollover value, matching the highest frequency of the landslide-area distribution, (2) the power-law scaling exponent, α , defined from the slope of the linear regression measured for large landslides events, and (3) the cutoff value, related to the divergence of the distribution from a power-law scaling. With the exception of Except for a few parameter combinations (in the range of tested parameters of friction and cohesion), the simulated landslideslandslide size-frequency distributions we obtained did not display any clear rollover. This lack of rollover is probably due to the coarse resolution of the grid (25 m) which makes it impossible to visualize small landslides. Therefore, we do not use this criterion for our model calibration approach. The power-law scaling exponent is a key parameter as it describes the frequency of intermediate to large landslides, which convey most of the eroded volume. This exponent also varies

significativelysignificantly with the internal angle of friction (Fig. 4B). As no power-law exponent value exists for the French Alps landslide-rockfall inventories, we use as a reference the mean value α_{mean} = -2.3 suggested by (Van Den Eeckhaut et al., 2007) Van Den Eeckhaut et al. (2007) from a global landslide compilation. (Tanyaş et al., __(2018, 2019) also carried out a landslide compilation and analysis of landslide size-frequency distributions, proposing a slightly higherlarger power-law exponent (α_{mean} = -2.5). However, this inventory only considers earthquake-induced landslides. In addition, power-law exponents tend to be smaller for igneous or metamorphic rock (such as present in our study area) (Bennett et al., 2012), so we retain the value of -2.3 for our model calibration. In our calibration phase, we set the cutoff area at 3- 10^4 m² based on the shape of the linear regression fit and the good value of the Pearson correlation coefficient (Fig. 4A). Our cutoff value seems to be smaller but overall consistent with previously reported values (Tanyas et al., 2018; 2019).

The simulated landslide size-frequency distribution (Fig. 4A), in a log-log plot, illustrates the decrease in landslide number when increasing landslide size. From all simulated landslides (5. 10^4 in total; see Section 3.2), we randomly select 20 000 landslides to construct the landslide size-frequency distribution. This method ensures a homogeneous number of events between different combinations of input parameters (Fig. 4B). Therefore, we compare the simulated power-law scaling exponent α , resulting from different combinations of cohesion (C) and internal friction angle (φ), with the literatureexpected power-law exponent of -2.3. The power-law regression is computed using a log-log linear fit. The output matrix (Fig. 4B) shows a gradient for the power-law exponent α with increasing φ values. In our simulations, α varies strongly, between -1.7 and -3.1, when changing the internal angle of friction (31-39°, Fig. 4B). This range is consistent with global compilations of power-law exponents for landslidearea scaling (Tanyaş et al., 2018, 2019; Van Den Eeckhaut et al., 2007). We also observe little variability in α with cohesion (C). Therefore, we fix the internal angle of friction at $\varphi = 35^\circ$ which leads to simulated values of α close to -2.3. As the cohesion parameter seems to not influence the power-law exponent of the landslides size-frequency distribution, we calibrate this parameter using an alternative strategy (see section 3.3.3).



|441

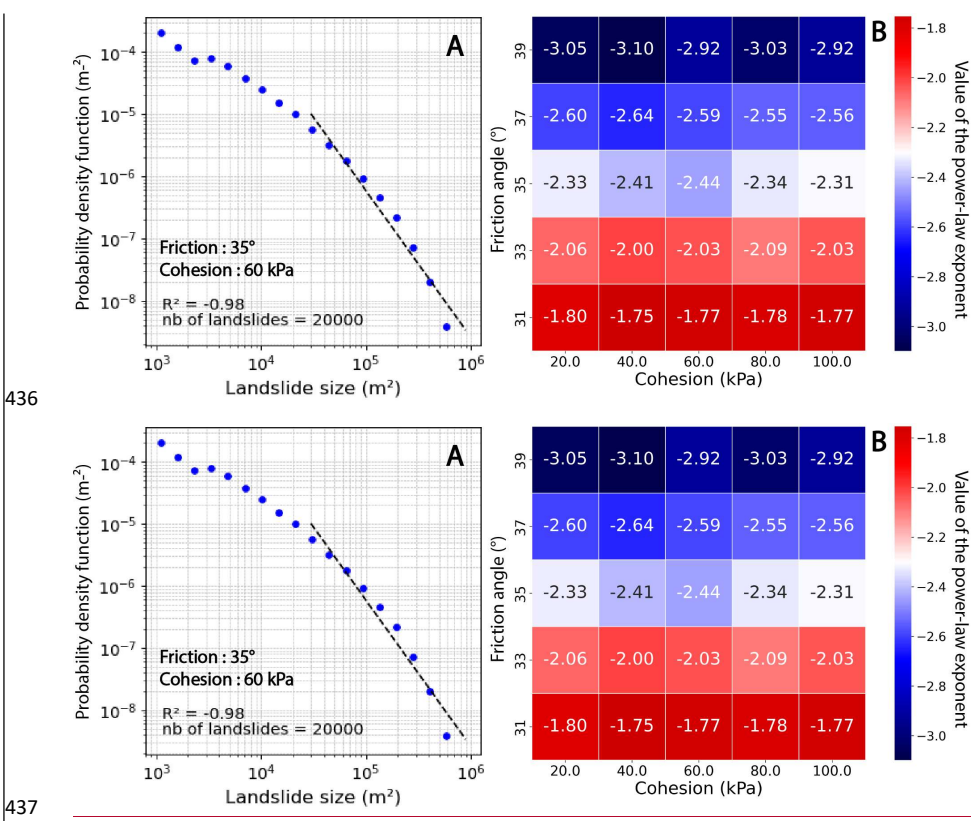


Figure 4: Calibration approach for the internal angle of friction and the cohesion in HyLandthe HyLands model. Calibration outcomes result from multiple simulations, with similar input parameters, to get a larger dataset of landslides (see text for discussion). A) Landslide size distribution, with a linear fit (dashed black line) on the power-law tail of the distribution. The cutoff value (i.e., minimum size where the linear fit starts) is set to 3: 10^4 m². B) Calibration matrix between the internal angle of friction (φ) and the cohesion (C). The angle of friction is calibrated based on the minimum difference between the power-law exponent of the simulated size distribution and the reference value (-2.3; van den Eeckhaut et al., 2007). Blue colors indicate output power-law exponents smaller than the reference value (-2.3, white colors) and red colors indicate predicted power-law exponents higher than the reference value.

As a verification of our model calibration, we also simulate the area-volume relationship for simulated landslide distributions (Fig. S1). The relevant cloud of landslides events ($n=\underline{=}426$) shows a power-law scaling similar to those observed elsewhere with an intercept value of 0.84 and an exponent value $\gamma=\underline{=}1.49$ (Fig. S1) (Larsen et al, 2010; Wood et al, 2015).

3.3.3 Calibration of landslide return time and cohesion: 10 Be-derived erosion rate

To calibrate the cohesion and the landslide return time parameters, we compare simulated and ¹⁰Bederived catchment-averaged erosion rates (3.2, Fig. 5). Both model parameters impact nonlinearly the

output erosion rate, and increasing t_{LS} or C leads to lower output decrease the resulting erosion rates (Fig. 5). Several combinations of parameters predict an outputa catchment-averaged erosion rated within the expected range (0.7 - 1.1 mm/yr): 1) a high C=100 kPa associated with a short $t_{LS}=80 \text{ kyr}$, 2) a small C=40 kPa associated with a long $t_{LS}=250 \text{ kyr}$, or 3); grey band). In the following, we use an intermediate parameter combination with, C==60 kPa and $t_{LS}==150 \text{ kyr}$. These three, as the different possible model parameterizations also(Fig. 5) lead to roughly similar spatial and temporal patterns in landslide activity. In the following, we therefore use the intermediate parameter combination (Fig. 5). We also ran simulations for two end-member parameter combinations: a minimum combination (C=20 kPa and $t_{LS}=50 \text{ kyr}$) and a maximum combination (C=100 kPa and $t_{LS}=250 \text{ kyr}$). Results show a strong variability in landslides frequency and associated erosion rates but a similar spatial landslide distribution (Fig. S2).



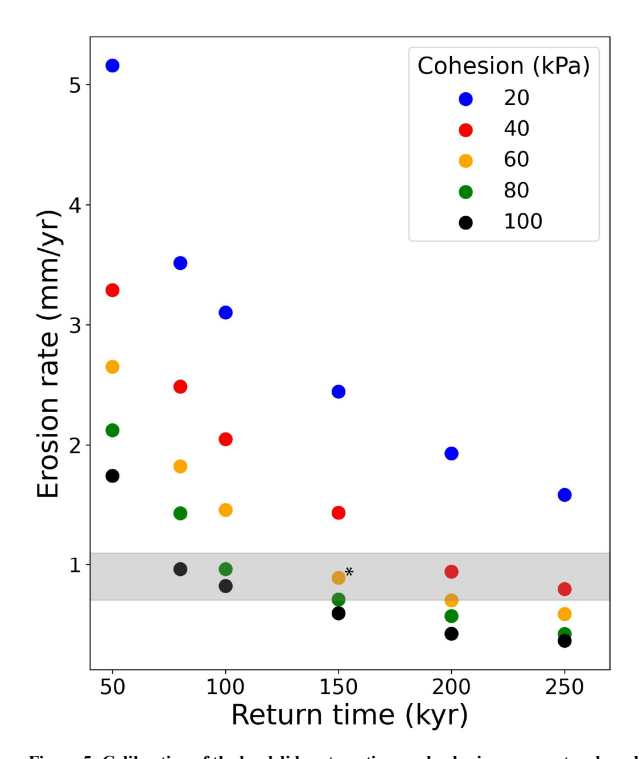


Figure 5: Calibration of the landslide return time and cohesion parameters based on the simulated catchment-averaged landslide erosion rate. Considering the calibrated angle of internal friction (35°, Fig. 4B), each dot represents a particular combination of landslide return time and cohesion (color code indicating the cohesion value). The selected combination is identified with a starsstar (*). The simulated erosion rate is an averaged catchment-scale erosion rate over a compilation of 20 different simulations (1500 yr duration). The grey band illustrates the range of observed erosion rates from the literature-values (0.7-1.1 mm/yr; Delunel et al., 2010).

4. Results

476

477

478

479

480 481

482

483

484

485

486

487

488

489

490

491

492

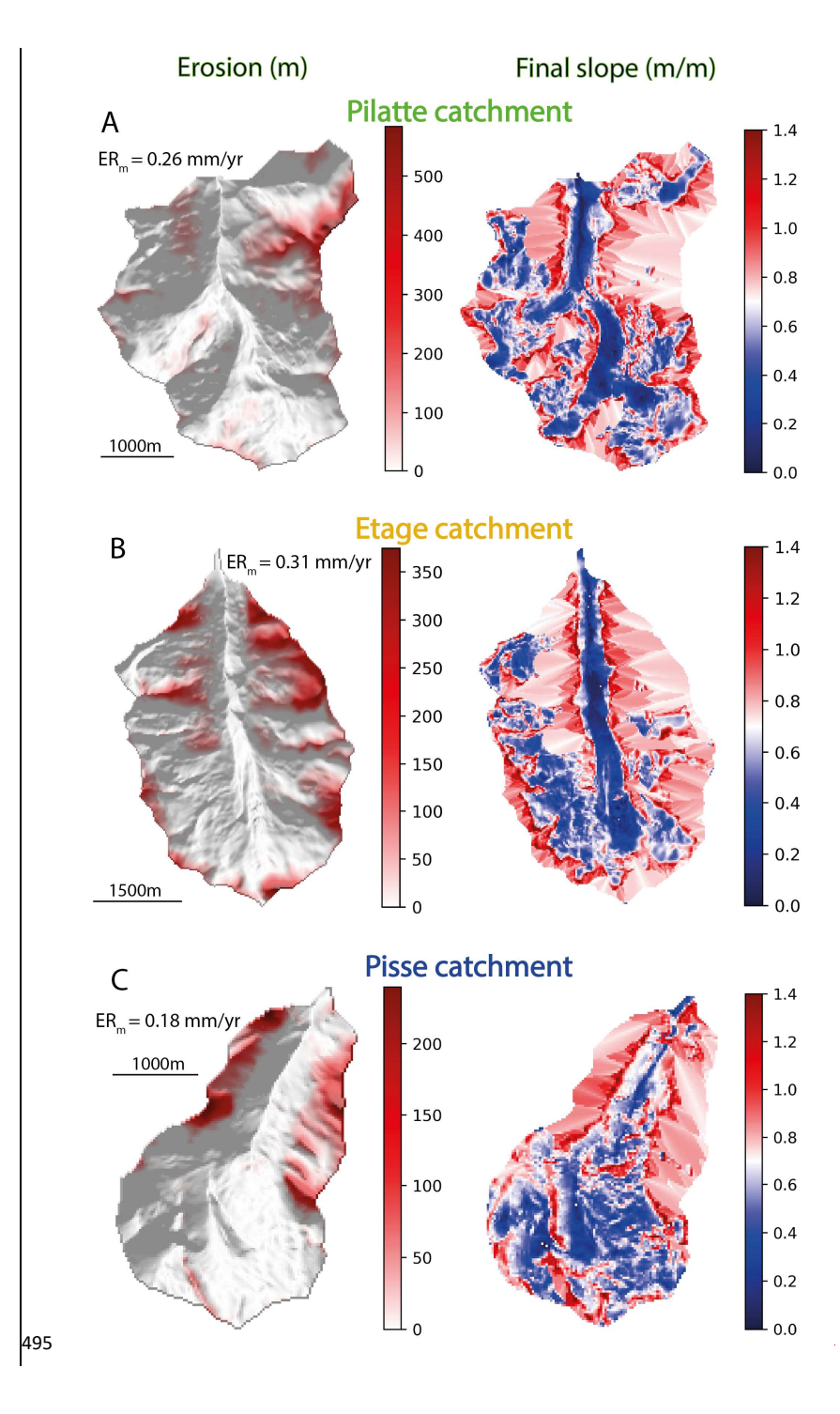
493

494

4.1 Spatial and temporal distribution of landslide activity

Using the calibrated model, we investigate the impact of landslide activity on catchment topographic changes over 100 kyr (timescales fortime scales representing glacial-interglacial cycles). Over this timescale, the calibrated landscape evolution model generates different spatial patterns of landslide erosion across the three studied catchments (Fig. 6). In each catchment, landslide erosion is distributed heterogeneously, ranging from areas experiencing an intense landslide activity and significant topographic changes to overall unaffected areas. For the Pilatteglacial catchment (glacialPilatte), significant topographic changes, up to 500 m, occur along its northeast ridges. Elsewhere, predicted landslides lead to smaller topographic changes, of up to around 100 m (Fig. 6A). The intermediate glacial-fluvial catchment (Etages) shows erosion patches along its crests and summit walls. In some areas, eumulated cumulative erosion reaches 350 m, while shallower landslides smaller cumulative landslide erosion are observed on low-elevation hillslopes, just above the valley bottom (Fig. 6B). For the Pissefluvial catchment (fluvialPisse), landslide erosion is mainly focused on the downstream parts of the catchment where the valley narrows and slopes become steeper. CumulatedCumulative landslide erosion reaches up to 250 m, however, but the upper part of the catchment shows limited landslide activity (Fig. 6C). The final slopesdistributions of slope across the three catchments clearly highlight the locus of landslide activity. Indeed, landsliding results in homogeneoushomogenizing slopes which only slightly exceedsabove the internal angle of friction (i.e., 0.7, represented by white color in Fig. 6).

Formatted: Outline numbered + Level: 1 + Numbering Style: 1, 2, 3, ... + Start at: 1 + Alignment: Right + Aligned at: 0,5 cm + Indent at: 1,13 cm



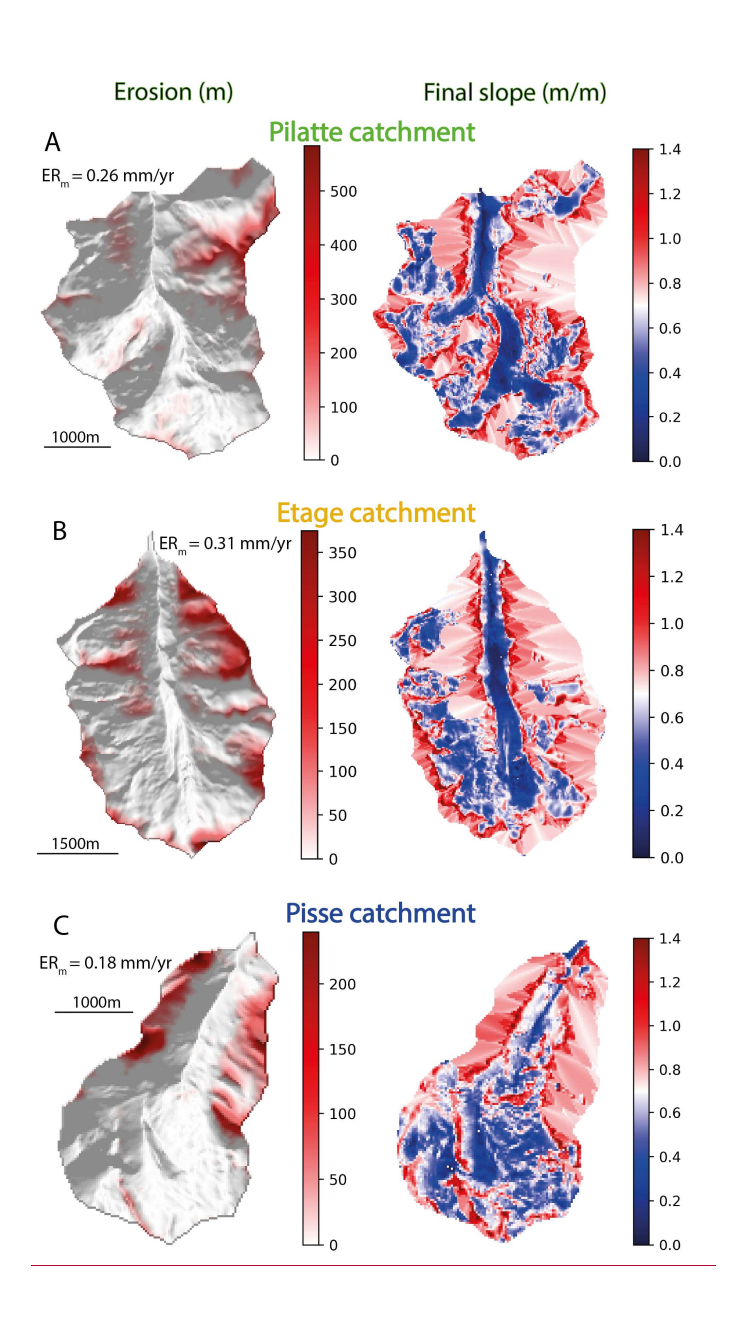


Figure 6: Simulation results of cumulative landslide erosion and final slope distribution for the studied different catchments (A - Pilatte, B - Etages, C - Pisse). Left panels display landslide erosion patterns with cumulative landslide erosion (red color) over 100-kyr simulation duration on the modern hillshade DEM. The catchment-averaged mean erosion rate is indicated (ER_m) Right panels show the final slope distributions where the landslide activity results in more homogenous slope patterns around the input internal angle of friction (0.7 m/m, white colors).

499 |500 |501 |502

504

505

506 507

508

509

510 511

512

513

514

515

516

517

518 519

520

521

522 523

524

525

526

527

528

529 530

531

532

533

535

4.2 Spatial distribution location of landslides landsliding

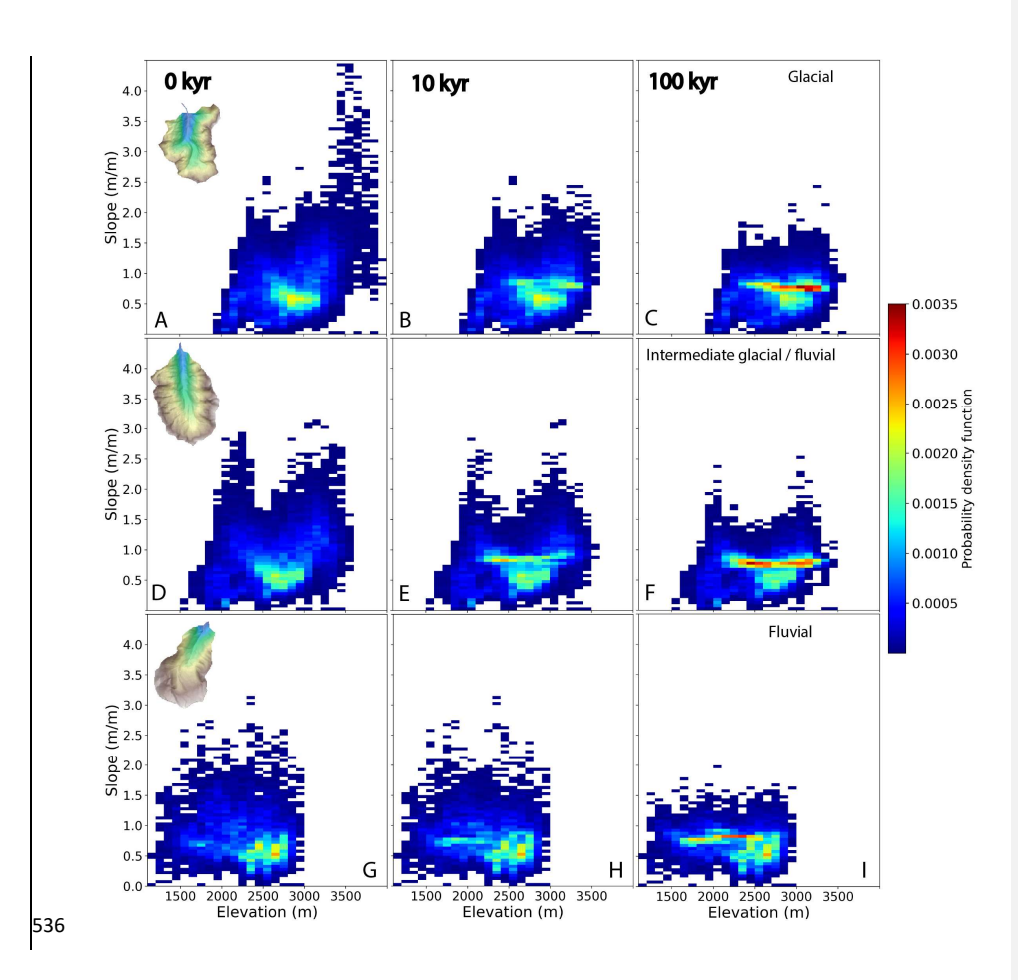
For each catchment, we investigate the simulated evolution of both the hypsometrichypsometry and topographic slope distributions (i.e. 2D histograms of catchment slope and elevation, Fig. 7A,D,E). As expected from the modern slope distribution (Fig. 1C), the initial catchment topographies (i.e., at 0 kyr) show a similar modal slope around 0.6 m/m. This modal slope is reached at different elevations for the different catchments: 2800, 2600 and 2600 m a.s.l. for the glacial, intermediate glacial-fluvial and fluvial catchment, respectively (Fig. 7A,D,G). The initial model topographies of the glacial Pilatte (glacial) and Etage (intermediate glacial-fluvial (Etages) catchments show a bimodal distribution of the elevations for steep slopes (Fig. 7A,D et 8) (Fig. S3).

The steepest slopes of the glacial (Pilatte) catchment range between 2 and up to 4.5 m/m (i.e between ~63 and 77°) and are mostly restricted to the highest elevations (3000- 4000 m) (Fig. 7A). A second peak of steep slopes, with lower magnitudes (1.5 up to 2.5 m/m i.e \sim 56° 68°), is found around 2400 m. The intermediate glacial-fluvial (Etages) catchment also shows an initial topography with two similar 'peaks' of steep slopes frequency (Fig. 8C). We observe maximum slopes around 3 m/m (\sim 70°) between 2700 and the catchment crestline (~3500 m), and in a narrower elevation range from around 2000 to 2400 m (Fig. 7D). On the contraryIn contrast, the fluvial (Pisse) catchment differs from the other eatchments due to the relativein having a relatively homogeneous distribution of slopes with elevation (Fig. 7G; Fig. S43). Throughout the simulations, catchment slopes exceeding the friction angle at 0.7 m/m are affected by landslides, especially in the glacial catchment where significant changes can be noticed already after only 10 kyr simulation (Fig. 7B,E). Overall, after 100 kyr simulation, landslide activity has erased most of the steep slopes (almost three timetimes less steep slopes, for high elevations, at the end of the simulation, Fig. 8C)-1, i.e. above ~1.5 m/m, reducing significantly in turn the bimodal distribution of elevation for the steepsteepest slopes (Figs. 7C,F & and 8C). The maximum catchment elevation has decreased for the glacial and intermediate glacial-fluvial catchments, while it remains

During the simulations, we also observe a progressive increase in slope frequency slightly below 1 m/m (i.e_{5..} 45°), concentrated around 2600 - 3200 m, 2400 - 3000 m and 1900 - 2600 m for the glacial, intermediate glacial-fluvial and fluvial catchments, respectively (Figs. 7C,F,I & 8B). This new slope distribution evidences the shift from the initial steep slopes to final intermediate slopes that are closer

approximately constant for the fluvial catchment after 100 kyr of simulation.

534 to the input internal friction angle.



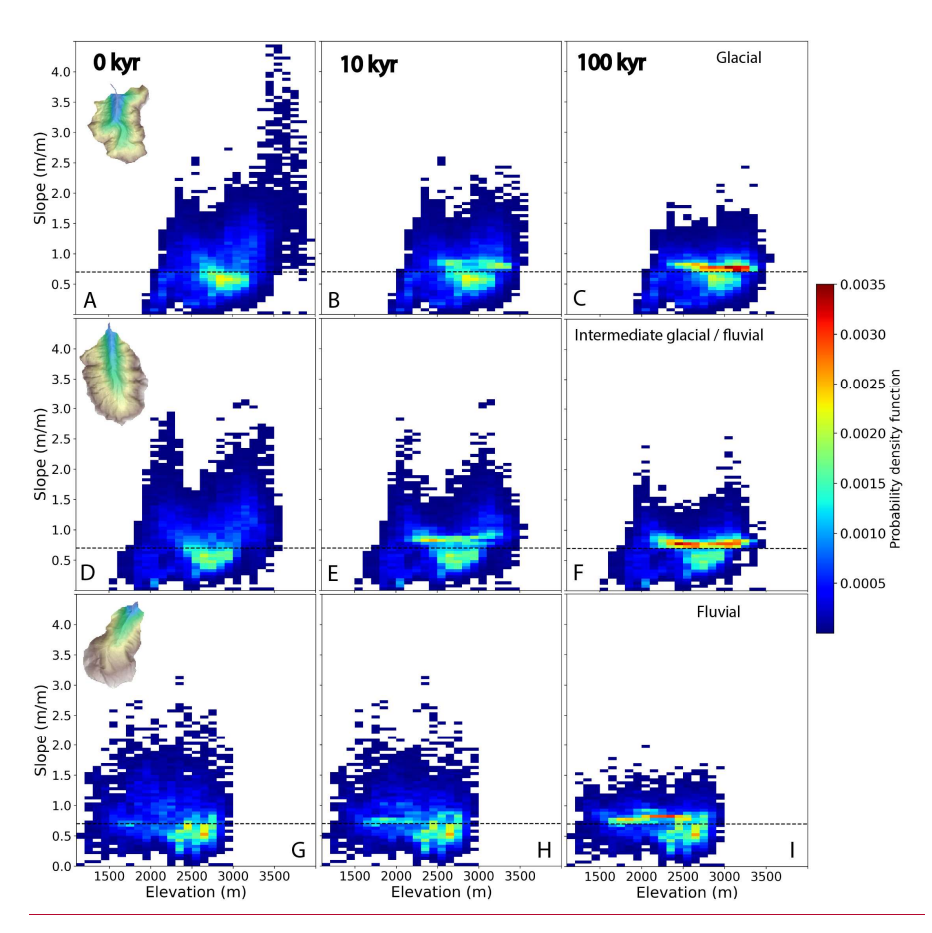


Figure 7: 2D histograms of the catchment slope distributions (color scale) with elevation. The temporal evolution of eatehments catchment slopes and elevations during simulations is monitored at three different time steps: 0, 10, anand 100 kyr (left, middle and right, respectively). Each row shows model results for a particular catchment: glacial (Pilatte (glaciated, A-B-C), Etages (intermediate Intermediate glacial-fluvial (Etage, D-E-F), and Fluvial (Pisse-(fluvial, G-H-I). For all three catchments, steep slopes are erased and catchment slopes tend toward more homogeneous slopes around and just above the input internal angle of friction (0.7 m/m, i.e. 35°).

538 |539 |540 |541 |542 |543

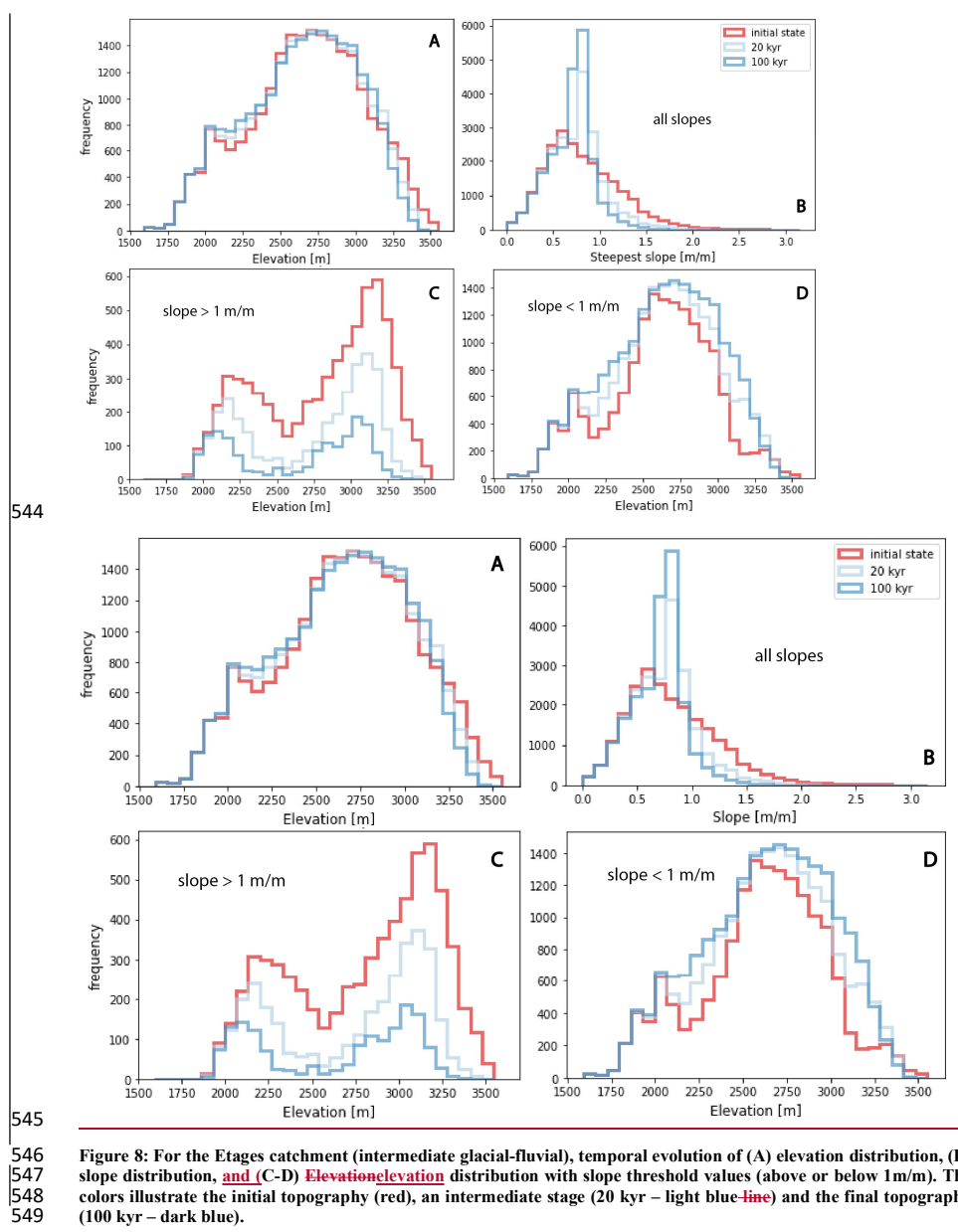


Figure 8: For the Etages catchment (intermediate glacial-fluvial), temporal evolution of (A) elevation distribution, (B) slope distribution, and (C-D) Elevationelevation distribution with slope threshold values (above or below 1m/m). The colors illustrate the initial topography (red), an intermediate stage (20 kyr – light blue—line) and the final topography (100 kyr - dark blue).

4.3 Temporal distribution of landslides

550 551

552

553

We now investigate the relationship between topographic changes and landslide activity (Fig. 9). Here, we identify each landslide by its time of occurrence and its triggering location, corresponding to its lowest elevation (Fig. 9). First, our results highlight the bimodal elevation distribution of the simulated landslides, roughly above 2800 m and below 2400 m, which appears persistent with time for the glacial and intermediate glacial-fluvial catchments (Fig. 9A,B). These two catchments also show an intense landslide activity for the first 20 kyr of simulation, with an apparent progressive decay with time. Large landslides occur throughout the 100 kyr of simulation time, illustrating the stochastic nature of landslide occurrence in HyLands-simulations. These observationsmodel predictions are supported by the cumulative distribution of landslides volume through simulation time (Fig. 10A-C). For the glacial and intermediate glacial-fluvial catchments, more than half of the total landslide volume is predicted before 20 kyr. However, the cumulative number of landslides increases with time for these catchments. This discrepancy between the total landslide volume and the number of landslides may illustrateillustrates the preferential occurrence of large landslides within the first 20 kyr. This interpretation is supported by the change in the probability density function of the landslide volumes after 20 kyr simulation time (Fig S5). For these two (intermediate) glacial catchments, the difference in the exponent of the power law scaling indicates the higher frequency of large landslides within the 20 kyr of simulation time (Fig 7G-H).S54). We do not observe this pattern for the fluvial catchment (Fig S54 C, F), although the largest landslides are still predicted during the first 20 kyr of simulation time. Another interesting result is the inverse relationship between the predicted landslide volume and the number of landslides at different catchment elevations: at low elevations (<2700 m), landslides are less frequent but large landslides are overrepresented; whereas at high elevations (>2700 m), landslides are more frequent but large landslides are underrepresented. This assessment is particularly true for the glacial (Pilatte (glacial) and Etages (intermediate glacial-fluvial (Etage) catchments (Fig. 10A-B). For instance, the Pilatteglacial catchment (Fig. 10A) displays twice moreas many landslide occurrences at high elevations (>2700 m), with only a slightly larger eroded volume above than below 2700 m elevation. Observations are significantly different for the fluvial catchment as the landslides are rather homogeneously distributed in the catchment (Fig. 9C). However, the high occurrences of landslides in the first 20 kyr are still noticeable (Fig. 10C) and large landslides tend to occur preferentially at low

554

555

556

557

558

559560

561

562

563564

565

566

567

568569

570

571572

573

574

575

576

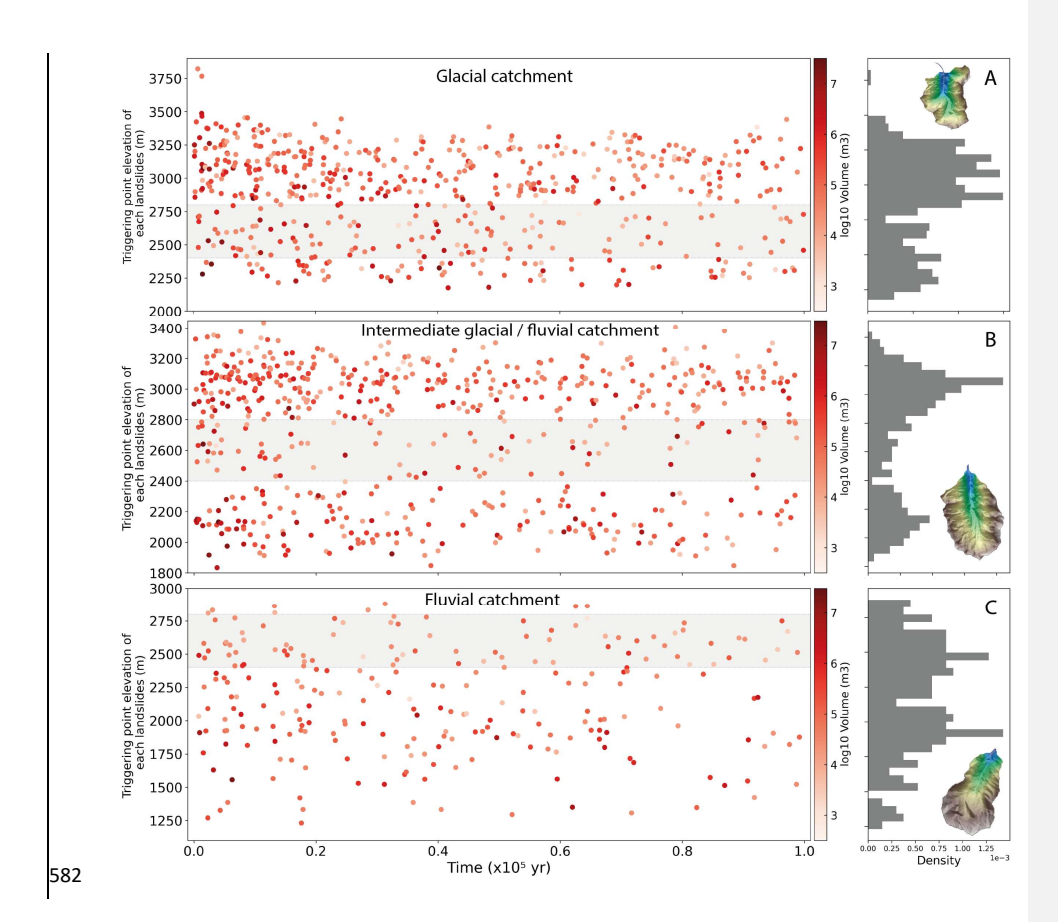
577

578579

580

581

elevation (<2200 m).



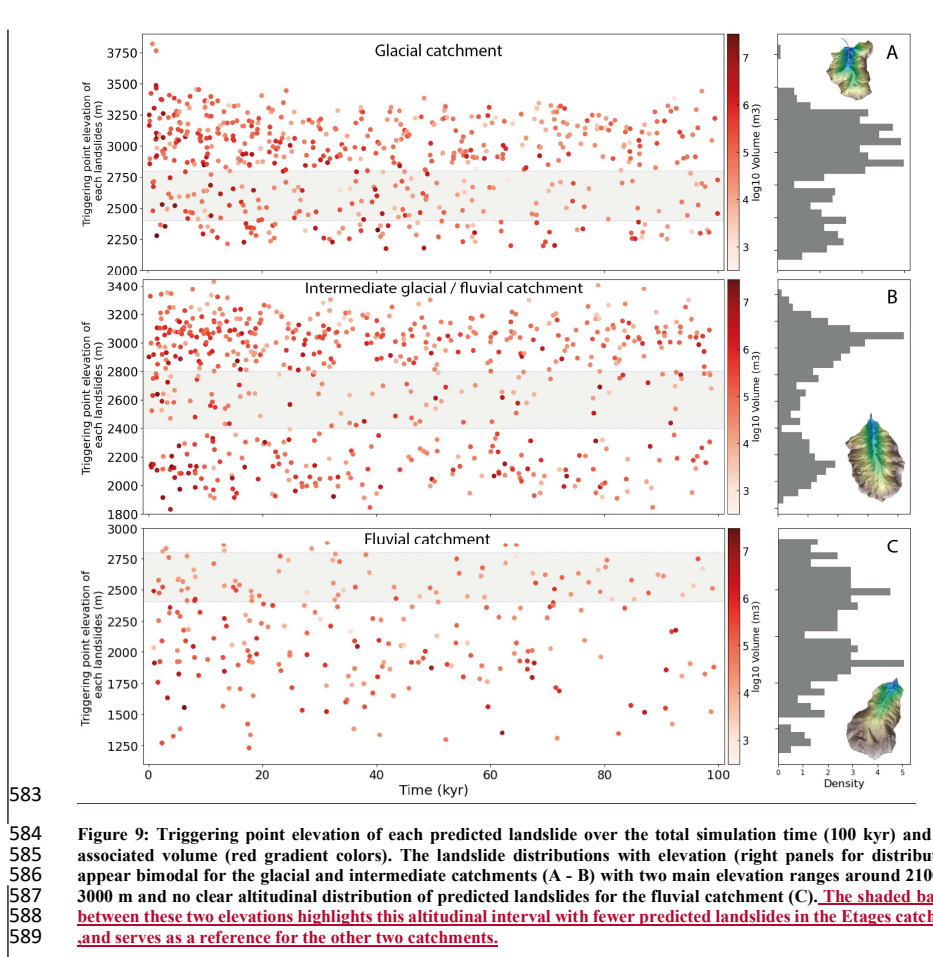


Figure 9: Triggering point elevation of each predicted landslide over the total simulation time (100 kyr) and their associated volume (red gradient colors). The landslide distributions with elevation (right panels for distributions) appear bimodal for the glacial and intermediate catchments (A - B) with two main elevation ranges around 2100 and 3000 m and no clear altitudinal distribution of predicted landslides for the fluvial catchment (C). The shaded band in between these two elevations highlights this altitudinal interval with fewer predicted landslides in the Etages catchment and some one wife groups for the other time sets hands. ,and serves as a reference for the other two catchments.

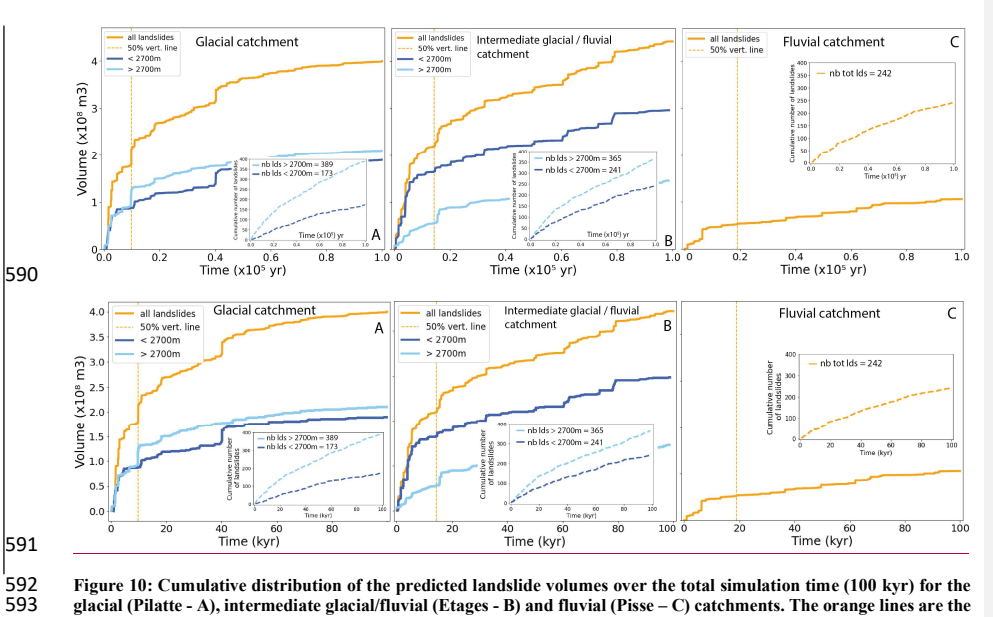


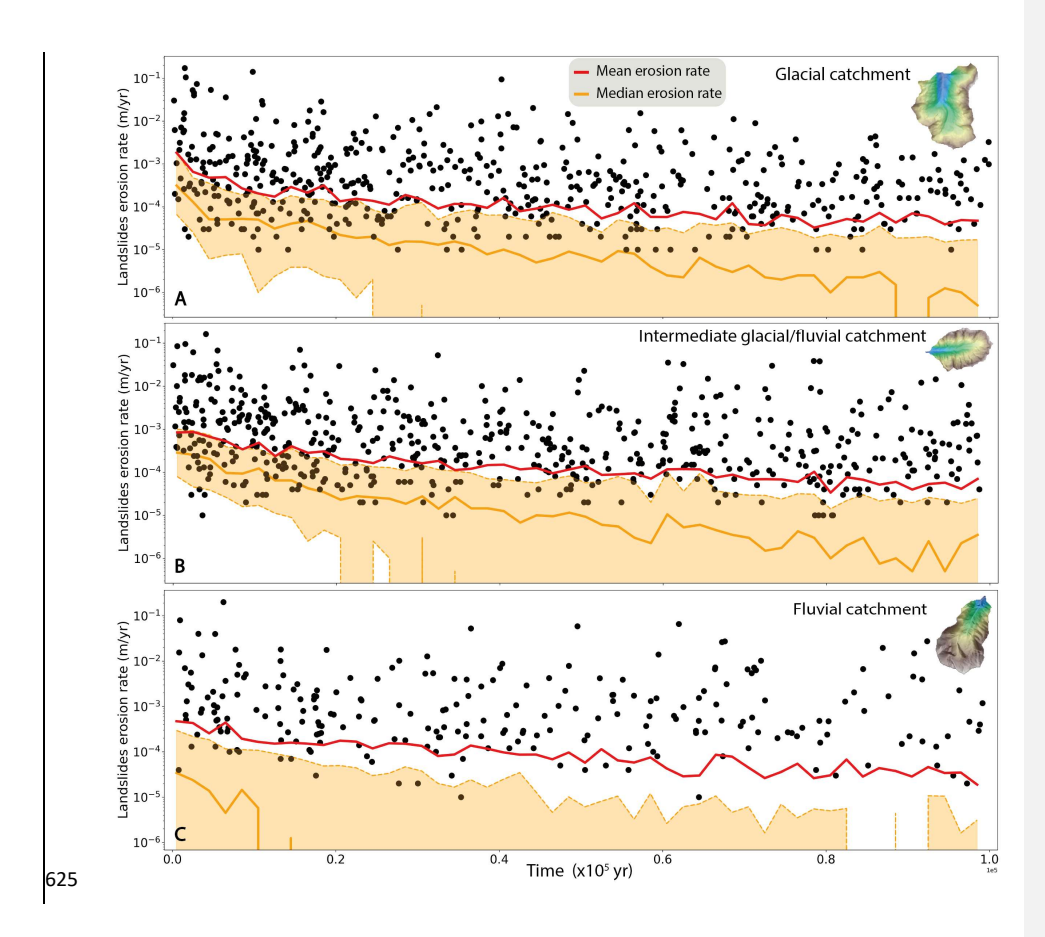
Figure 10: Cumulative distribution of the predicted landslide volumes over the total simulation time (100 kyr) for the glacial (Pilatte - A), intermediate glacial/fluvial (Etages - B) and fluvial (Pisse - C) catchments. The orange lines are the total cumulative landslide volumes, while the blue lines display the predicted cumulative volumes for landslides located above (light blue) and below (dark blue) an elevation threshold of 2700 m. The yellow vertical dashed lines indicate the simulation time when 50% of the total landslide volume is reached. Insets show the cumulative number of landslides generated during the simulation time for the two defined elevation classes.

4.4 Temporal evolution of landslide erosion rate

The term 'erosion rate' describes here only the predicted erosion induced by landslides and averaged over the catchment area. For each studied catchment, we compute the evolution of the catchment-averaged erosion rates using a 2-kyr time window, providing different statistics: mean, median, 25th and 75th percentiles of catchment-averaged erosion rates (Fig. 11). This temporal window emphasizes the general long-term trend of the predicted erosion rate by smoothing its high-frequency variations related to the stochasticity of landslide occurrence (Fig. S65). For all three catchments, the catchment-averaged erosion rates vary roughly between 10⁻⁵ and 10⁻¹ mmm/yr when at least one landslide is triggered during the time window. The predicted mean erosion rate is always significantly higher than the median erosion rate (almost 10 times at the beginning of the simulation and around 100 times after 100 kyr of simulation time), but the same progressive decreasing trend is observed for both two statistical measures. In addition, the 25th percentile rapidly becomes null, highlighting that the catchment-averaged erosion rate is driven by large but infrequent landslides.

The glacial (Pilatte (glacial) catchment (Fig. 11A) shows a particular high mean erosion rate, above 1 mm/yr, with a rapidly decreasing trend during the first 10 kyr. Then, the mean erosion rate decreases more slowly until 60 kyr and getsbecomes roughly constant at 0.1-0.2 mm/yr over the last 40 kyr of simulation. A similar trend is observed for the Etages (intermediate glacial-fluvial catchment (Etages,

Fig. 11B), but the initial erosion rate is ~1 mm/yr and apparently-lower than for the glacial (Pilatte (glacial) catchment. Onln contrast, the contrary, the Pisse (fluvial (Pisse) catchment (Fig. 11C) shows a progressive decrease in the mean erosion rate, from ~0.6 to 0.06 mm/yr after 60 kyr of simulation, with no observed peak in erosion rate at the beginning of the simulation. The median value for the fluvial catchment reaches rapidly zero within the first 20 kyr of simulation, illustrating the lower frequency of landslide occurrence compared to the glacial and intermediate glacial-fluvial catchments. Overall and for all studied catchments, predicted landslide erosion rates decrease by about an order of magnitude over 100 kyr, illustrating the progressive erasing of steep slopes associated to glacial morphological features.



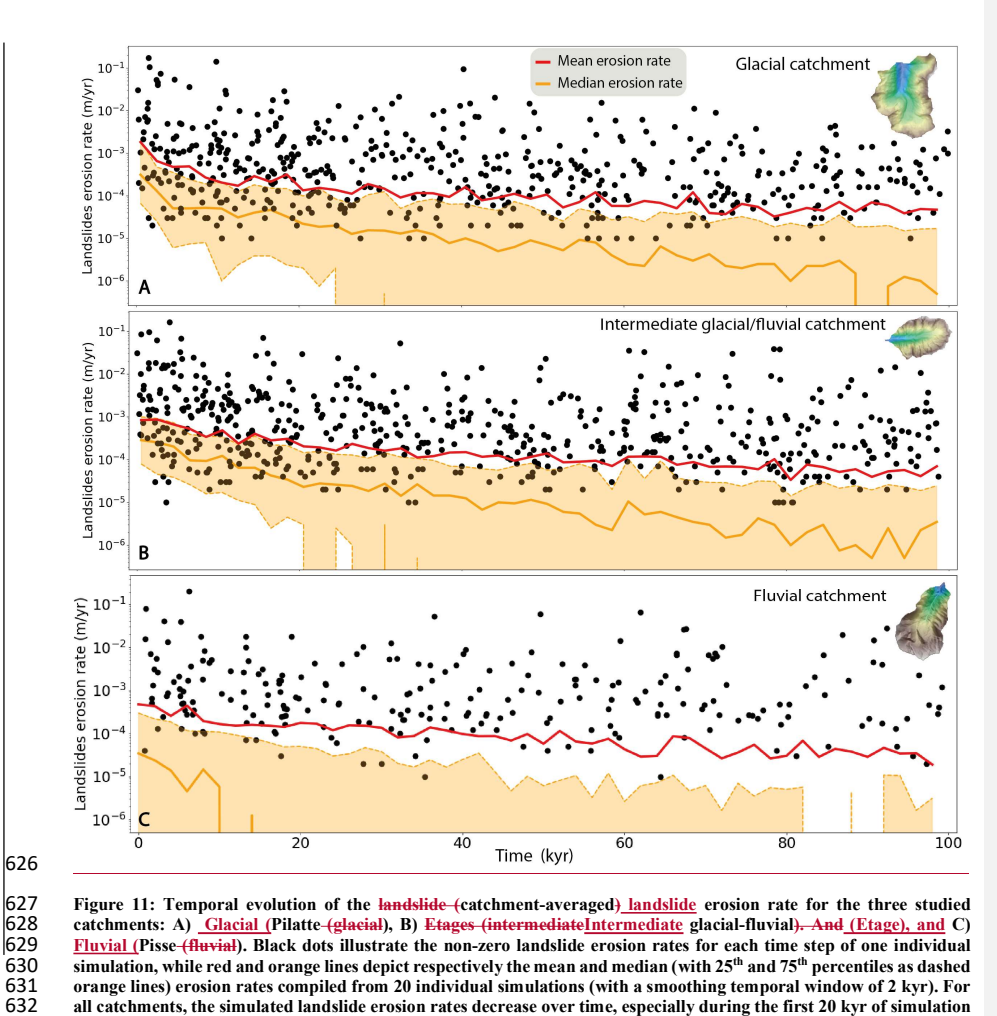


Figure 11: Temporal evolution of the landslide (catchment-averaged) landslide erosion rate for the three studied catchments: A) Glacial (Pilatte (glacial), B) Etages (intermediate Intermediate glacial-fluvial). And (Etage), and C) Fluvial (Pisse (fluvial). Black dots illustrate the non-zero landslide erosion rates for each time step of one individual simulation, while red and orange lines depict respectively the mean and median (with 25th and 75th percentiles as dashed orange lines) erosion rates compiled from 20 individual simulations (with a smoothing temporal window of 2 kyr). For all catchments, the simulated landslide erosion rates decrease over time, especially during the first 20 kyr of simulation time, with different temporal trends depending on the catchment.

Discussion

633

634

635

636

637

638

639

640

641

642

5.1 Model limitations Modeling approach

Our landscape evolution model using HyLands has been designed to explore the hypothesis that landsliding represent a dominant geomorphological agentimpact of landslide activity in reshaping alpine landscapes during postglacial periods. Our numerical simulations succeed in reproducing a pulse of landslides activity during the postglacial period and its complex (non-homogeneous) impact on catchment hypsometry and slopes. However, this reduced-complexity model represents a simplified version of real hillslope dynamics, with limitations regarding its ability to predict in details all the

Formatted: Outline numbered + Level: 1 + Numbering Style: 1, 2, 3, ... + Start at: 1 + Alignment: Right + Aligned at: 0,5 cm + Indent at: 1,13 cm

richness of natural landforms, especially under the constraint of long simulation time (Tucker & Hancock, 2010). (Tucker and Hancock, 2010). Therefore, we made several modeling choices (see Sections 3.2 and 3.3) to minimize potential feedback loops and interaction between erosion processes, which may have impacted our results as discussed below.

5.1.1 Missing processes: rock uplift, -fluvial erosion and sediment transport

643

644

645

646 647 648

649 |650

651 652

653

654

655

656

657

658

659

660

661

662

663

664

665

666

667 668

669

670

671

672

673 674

675

676

677

As mentioned earlier, the model does not account for the impact of uplift, which can be considered as a limitation. Given the present-day rock uplift rate in the western European Alps, around 1 mm/yr (Nocquet et al., 2016; Sternai et al., 2019), the total uplift over the simulation period (100 kyr) would be around 100 m. This theoretical uplift value is of the same order of magnitude than the average decrease in elevation caused by landslide erosion in the Etages (intermediate glacial-fluvial (Etages) and Pisse (fluvial (Pisse) catchments (Figs. 6-7). In the glacial (Pilatte (glacial) catchment, the mean erosion is around 26 m, with maximum cumulated erosion of ~500 m. Therefore, integrating rock uplift in the model, from either geodynamics, tectonic activity or glacial isostatic rebound (Sternai et al., 2019), could counterbalance the overall decrease in catchment elevation observed in our results. Indeed, postglacial rebound can occur at km scale, promoting local rock uplift and potentially considered to be a significant factor in triggering landslides in some regions (É. Cossart, 2013). (Cossart, 2013). In addition, rock uplift has also been proposed as modulating the post-glacial geomorphic response and landscape transition from glacial to fluvial states (Prasicek et al., 2015), rock upliftby allowing faster relief turnover times. In addition to uplift, tectonic activity could be associated with seismicity, another well-known triggering factor for landslides (Keefer, 1984; McColl, 2012). However, ourdespite these limitations, we believe that our modeling approach stays appropriate to assess the hillslope stability over 100-kyr timescales, which is largely dependent on climatically-shaped alpine topography, inherited from glacialinterglacial cycles, and bedrock mechanical strength. The impact of local earthquakes would mostly result in changing the timing of landslide activity, not the total volume of landslides. The catchment-averaged erosion rate of 1 mm/yr, derived from published cosmogenic nuclide data (Delunel et al., 2010) and used for the return time calibration, is integrating a large fluvial network with multiple erosion processes (fluvial, hillslope, landslide) at the scale of the Ecrins massif. Considering effective sediment connectivity in the catchment (in our study area, main fluvial valleys are sediment bypass areas without significant incision but potential transient storage) and only landsliding to derive our catchment erosion rate, 1 mm/yr is likely to be an end member minimum value for our simulations. Therefore, we ran a supplementary simulation with a lower cohesion value (20 kPa) while keeping the same return time (150 kyr), leading overall to a higher erosion rate (about 2-3 mm/yr, Fig. 5). The simulation results show a globally higher frequency of landslides, but with similar patterns in landslide occurrence, topographic changes and temporal trend in erosion rate (Fig.S76).

Finally, we did not include fluvial erosion and sediment export in our simulations. Ignoring sediment transport over either the postglacial period or a long timescale (100 kyr), integratingwhich in reality should include multiple glacial-interglacial periodsoscillations, is a strong model limitation for alpine erosion dynamics (Schlunegger & Hinderer, 2003). Indeed, sediment transfer dynamics over the Quaternary period is(Schlunegger and Hinderer, 2003). Indeed, sediment transfer dynamics over the Quaternary period are associated with glacial dynamics (Antoniazza & Lane, 2021)(Antoniazza and Lane, 2021), coupling between hillslopes and channels (Hovius et al., 2000), local fluvial incision (Leith et al., 2018; Valla et al., 2010) and potential transient sediment storage (Buechi et al., 2018). Rivers are also considered as the main agent of sediment transport during interglacial period (M. N. Koppes & Montgomery, 2009; Pitlick et al., 2021). (Koppes & Montgomery, 2009; Pitlick et al., 2021). Fluvial incision also leads to a lowering of the base level, which in turn creates more steep slopes at the hillslope foottoe. These changes participatecombine to renew the landslide potential of these transient landforms. However, in this study we modeled a single interglacial period and provideprovided a focus solely on hillslopes dynamics (i.e., no fluvial dynamics); both arguments result in a lower influence of the sediment dynamics for our results.

5.1.2 Model parameterization parameterization

Our modeling strategy and parameterization have inherent limitations, such as our initial input DEM+ (modern alpine topography) with a low resolution (25 m). Such resolution allows long simulation periods in a reasonable simulation time with the capability to still capture first-order erosion processes and topographic changes (Campforts et al., 2022). However, this relatively low resolution may hinder potential the presence of small-scale topographic roughness that could influence both landslide occurrence and magnitude. In addition, we ran our model simulations over 100 kyr, which is longer than any interglacial period during the Quaternary. This particularly long duration enables to constrain the timescale required for the decay of landslide activity, until reaching a state of hillslope stability at the catchment scale. The model duration of 100 kyr is not a realistic timescale for a post-glacial phase. However, it is an interesting and necessary duration which enables 1) to assess clear temporal trends of erosion rates, smoothing out landslide variability, and 2) to quantify the duration required to reshape the glacially-inherited topographic imprints and to reach stable catchment hillslopes.

Moreover, we consider the present-day topography of the studied catchments to start the post-glacial simulations and to perform our model calibration. Yet, these landscapes have likely been already subject to post-glacial hillslopes processes and landsliding since glacier retreat, limiting the number of hillslope instabilities in the modern topographies. In turn, this means that the simulated rates of erosion at the beginning of the simulations are likely minimum values for representing post-glacial conditions. However, extrapolating further is difficult since deglaciation is asynchronous both between and within the studied catchments: the U-shaped valley floors and walls, at rather lower elevations, are the first

Formatted: Font: 11 pt

Formatted: Normal (Web)

Formatted: Font: 11 pt

Formatted: Font color: Accent 1

areas to have experienced landsliding, while higher-elevation areas such as ridges and cirques can be protected from instability for longer thanks to active permafrost and only recent glacier retreat.

714

715

716 |717

718

719

720 721

722

723 724

725

726

727

728

729

730

731 732

733 734

735

736

737

738

739

740

741

742

743

744

745

746

747

748

749

Another strong assumption is to ignore sediment deposition on the resulting simulated topography. Landslides are among thathe most efficient processes for producing sediments (Keefer, 1984) in mountainous areas, which can then be available for transport from hillslopes to the drainage network. The sediment connectivity (Cavalli et al., 2019), especially for bedload sediment, from hillslopes to channels is a key indicator to quantify sediment yields and morphological changes along the source-tosink profile (Comiti et al., 2019; Hooke, 2003; Lane et al., 2017; Micheletti et al., 2015). Thus, we explore the potential feedbacks of sediment deposition on landslide activity by testing the Hylands model with a null fine fraction parameter (Ff = 0), i.e. with a complete storage of landslide-produced sediment in the catchment. CoarseIn that case, coarse sediments are spread over the hillslopes, i.e. downstream of the landslide source, following a non-linear and non-local deposition law (Carretier et al., 2016). This deposition term depends on the transport distance which is driven by the critical slope, settled here equal to the tangent of the angle of internal friction (φ) (Campforts et al., 2022; Carretier et al., 2016). This new setup is the opposite of our main analysis (Ff=1, Section 3.2), where we assumed a perfect sediment connectivity within the catchment, leading to instantaneous sediment export (Fig. S8- $\underline{S9}$). Simulated sediment storage in the catchment (Ff = 0) causes a slight increase in landslide occurrence, especially at low elevations (<2700 m). We interpret this increase as a remobilization of the sediment deposits, which results in new landslide locations compared to previous simulations. The simulated deposition patterns are indeed mainly located in the valley bottom (Figs. S7 8). When the slopes of the deposits become greater than the internal angle of friction (0.7m/m, i.e. 35°), landslides can then occur. These landslides trigger in the sedimentary cover may also explain the slight landslides increase in the shouldering elevation zone (2400 – 2800 m, Figs. S7-8). However, the spatio-temporal landslide activity remains roughly similar to our previous simulations. Note that we have not computed the denudation rate without exported fine sediment because it would not be possible to compare it with the measured value.

Finally, our model parameterization assumes spatially uniform model parameters both within and between the three catchments. We used a single set of calibrated cohesion and internal angle of friction values (Figs. 3-4), without differentiation based on lithology, vegetation cover, elevation or glacial cover. This assumption may limit the model capacity in capturing the complex terrain roughness of modern alpine modern topographies, which may be a factor in increasing rock resistance to slidinglandsliding in natural environments. For example, in our catchment, the effect of the tree cover at low elevations mayis not be apprehended byincluded in the model. Thus, the expected reduction in landslide occurrence due to root reinforcement or changes in soil moisture (Muñoz et al., 2016) is not simulated. In addition, the role of high-elevation permafrost, its spatial variability and temporal evolution, on landslide activity (Magnin et al., 2017), is not captured by our simulations.

5.2 The spatio Spatio temporal landslide activity over the Quaternary period

The glacial inheritance of the alpine landforms, with glacial cirques, U shaped and hanging valleys (Fig. 3), is still a current field of investigation in terms of their formation through multiple glacial cycles of the Quaternary (Seguinot & Delaney, 2021) and their persistence during post-glacial periods (e.g. Herman & Braun, 2008; Prasicek et al., 2015). The relative contribution of glacial and fluvial crosion to Quaternary relief evolution is still debated because of the difficulties to quantify crosion over glacial interglacial timescales (Fox et al., 2015; Shuster et al., 2005; Sternai et al., 2013; Valla et al., 2011). Moreover, some studies (M. N. Koppes & Montgomery, 2009; Leith et al., 2014, 2018; Montgomery & Korup, 2011) have argued that Late Pleistocene glaciations had only a limited impact on Alpine topography, recent alpine relief evolution being then mainly driven by fluvial and hillslope processes during interglacial. In this context, our numerical results bring some insights into the role of these hillslope processes in the transition from glacial to fluvial morphologies.

5.2.1 Spatial landslide distribution and glacial imprint

The present day catchment morphologies (Fig. The long-term glacial inheritance on alpine landforms (e.g., Penck, 1905; Anderson et al., 2006; Sternai et al., 2013; Seguinot and Delaney, 2021) and the relative contribution of glacial and fluvial erosion to the Quaternary relief are still debated, highlighting especially the impact of fluvial and hillslopes processes during interglacial period of the Late-Pleistocene glaciations (Koppes & Montgomery, 2009; Leith et al., 2014, 2018; Montgomery & Korup, 2011).

769 <u>2011)</u>

In this context, our numerical results bring some insights into the role of these hillslope processes in the transition from glacial to fluvial morphologies.

5.2.1 Spatial landslide distribution and glacial imprint

The present-day catchment morphologies (Fig. 2) leave no doubt about the significant role of the-glacial processes in shaping the investigated landscapes in the Ecrins massif (Fig. 1). However, our Our initial hypothesisquestion about the role of landslide activity and their potential capacity of landslides to erasereshape this glacial topographic inheritance over the last post-glacial period is only partly validated bycan be discussed in light of the simulation resultsoutputs.

First, the spatial landslide activity pattern (Fig. 9) reveals that the <u>parts of each catchment with the most obvious</u> glacial morphologies are more subject to mass wasting processes. The steep slopes generated by glacial erosion, along the U-shaped valley walls and at high elevation (crestlines and nunataks), produce a bimodal distribution of landslides with elevation, while the shouldering (Fig. 3), i.e., the gentler slope interval at mid-slope, <u>induces a weakis much less affected by</u> landslides activity. Therefore, our simulation results suggest that the transition from U-shaped to V-shaped valleys, as evidenced by the glacial (Pilatte) and fluvial (Pisse) catchments (Fig. 3), is highlighting the reshaping of the inherited

glacial landscape through hillslope processes. However, the bimodal distribution of landslides with elevation is still noticeable after 100 kyr of simulation time (i.e., roughly ten times longer than the deglaciationpost-glacial period-for the area). Moreover, the number of modeled landslides and their spatial clustering is still significant for the glacial and intermediate glacial-fluvial catchments compared to the landslide pattern in the fluvial catchment (Pisse), which shows a more uniform distribution of landslides on hillslopes (Fig. 9). Thus, if the landslide activity and its spatial distribution can be considered as indicators of the hillslopes transition, our modeling results suggest that the glacial and intermediate glacial-fluvial catchments have not yet completed their post-glacial transition after 100-kyr simulation.

Second, the landslide volume distributions also illustrate a specific dynamics of mass wasting events in formerly glaciated catchments. For the upper catchments (glacial and intermediate glacialfluvial), our modeling results suggest that **modeled** landslides are more frequent at higher elevations, near the crestlines, than at lower elevation near the valley bottoms (Fig. 10). This 10). As we are working with a real initial topography (present day), influenced by permafrost, this result is consistent with the recent deglaciation of the upper catchments. Indeed, nunataks and crestlines in this interior part of the massif may still benefit from the stabilizing role of permafrost; and have not been impacted by landslides yet. Thus, the higher elevations of the catchment (i.e., above the trimline) still display steep and sharp slopes. Under a warming climate and the degradation of permafrost, these high-elevation and steep hillslopes will potentially be more and more prone to periglacial erosion processes (as it is already the case for the intermediate glacial-fluvial catchment). In parallel, our simulations predict large landslides at the lower elevations (Figs. 9 & 10). These results are consistent with the effect of debuttressing (i.e., stress variations resulting from glacial unloading) along the U-shaped valley wall following glacial recession (e.g., E. Cossart et al., 2008). This is also supported by the temporal clustering of the large landslides in the first 20 kyr. Yet, the occurrence of large landslides, due to their stochastic nature, remains occasional afterwards, which is consistent with other studies (Ivy-Ochs et al., 2017; Schwartz et al., 2017; Zerathe et al., 2014).

Therefore, the persistence of landslide activity in the glacial and intermediate catchments, even after long simulation times, highlights that hillslope processes such as landslides, in response to glacial topographic inheritance, may not be the only factor explaining the fluvial morphology observed in our downstream catchment (Pisse).

5.2.2 Temporal landslide activity and transient topography

Here, we discuss our initial hypothesis, that all the studied eatehments had the same glacial topographic imprint, and We show that the three catchments have a distinct modeled erosion dynamics explained by diachronous landslide activity following different glacial retreat times (Fig. 1). Following the previous spatial analysis (5.2.1), the observed temporal decrease in landslide occurrence and in predicted erosion rates over the first ~20 kyr (Fig. 11) reflects a decline in the proportion of unstable slopes during the

immediate post-glacial period. The faster erosion modeled at the beginning of the simulation for the glacial and intermediate glacial-fluvial catchments, (Fig. 11), compared to the fluvial catchment, highlights the role of landsliding as a main geomorphological agent during the transition from glacial to inter-glacial interglacial conditions. This initial and gradual pulse of erosion in the first 20 kyr of the simulation, which differs between the studied catchments, reflects the distinct topographic states with respect to landslide susceptibility. The glacial catchment (Pilatte) has not experienced intense periglacial processes, such as landslides, for a sufficiently as long period, resulting in this high erosion rate following debutressing of unstable glacial hillslopes (E. Cossart et al., 2008). (Cossart et al., 2008). The slowing down of erosion rates in the two upper catchments (glacial and intermediate glacial-fluvial) is also illustrating this long-term transitional stage, in which hillslope processes may continue to control sediment production, but at a smallerslower pace. With few landslides occurring at the end of our simulations, and associated to a low erosion rate, the Pisse (fluvial (Pisse) catchment could be considered at the end of its transient phase and close to "post-glacial topographic steady-state" dominated by hillslope processes (i.e., no to few slope destabilizations landslides). The modelled pulse of erosion for the postglacial phase implies that the Late Pleistocene period, marked by the transition from glacial to hillslope processes, has reactivated alpine landforms by reshaping new steep and unstable hillslopes along the U-shaped valleysvalley walls or in the cirque areas. With its These particular morphologies (Fig. 2), the resulting from glacial inheritance sustains, sustain the potential for landslide erosion-potential and may become an indicator of the glacial impact on alpine topographies. However, our model results also show that simulated landsliding over 100 kyr (duration exceeding the typical interglacial period) is not sufficient for the full transition from aerasing steep glacial to a fluvial steady-state topographymorphologies. Indeed, the simulated landslide activity - the bimodal landslide distribution (Fig. 9) - and the associated erosion rate are still significant at the end of our 100-kyr simulations, meaning that the hillslope system alone requires longer timescales than the typical Milankovitch cycle to reach a steady"interglacial-state" topography (i.e. a topography withoutwhere glacial imprint has been erased, no longer inducing hillslope instabilities). A longer simulation of 1 million years shows that a plateau is reached in the first 100kyr but that thethe modeled erosion rate reaches a plateau in the first 100 kyr but then gradually decreases gradually until 400 kyr (Fig. S109). At this This is the characteristic time, the probability of failure is so small (probably because of no slope above required to obtain stable hillslopes in the internal angle of friction), that absence of external forcing. Note that after a characteristic time, maybe more than 100 kyr, the landslide-derived erosion rate is final topography would result in a simple threshold slope model, close to zerothe critical slope. However, compared to a simple slope threshold model, the stochastic aspect of our model enables to

823

824

825

826

827

828

829

830

831

832

833

834

835

836

837 838

839 840

841

842

843 844

845

846

847

848 849

850

851

852

853

854

855

856

857 858

859

First, <u>results from</u> this <u>observationlong term simulation</u> can be compared to fluvial processes, which also have long timescales for reaching steady-state topographic conditions (Whipple, 2001). Since

describe both individual landslide distribution and their timing during a post-glacial period.

hillslope processes are also largely contributing to sediment production in alpine settings, the topographic response time to landsliding may play a role in the sediment cascade transfer cascade which in turn would influence fluvial dynamics and erosion rates. Second, this relatively long activity of the hillslope system during the interglacial period – calibrated from cosmogenic-nuclide derived erosion rates (section 3.3.3) - is also consistent with the absence of uplift and fluvial incision in our modeling approach. Including these model components in our simulations may decrease the duration of post-glacial landsliding activity for the studied catchments, with rock uplift promoting faster response of the hillslope-fluvial system as observed for natural settings (Prasicek et al., 2015).

Given the long persistence of landsliding from our simulations (>100 kyr), the observed differences in landslide activity between the glacial/intermediate and fluvial catchments cannot be fully explained by the time lag in glacier retreat and the duration of the interglacial period (~10 kyr, Fig. 1). We thus propose that the glacial imprint may have been less intense in the fluvial (Pisse) catchment than in the glacial and intermediate glacial-fluvial catchments (Pilatte and Etages). This confirms), which could be explained by the more external position of the catchment in the massif and its overall lower elevations. This is consistent with the non-uniform impact of glacial processes on mountainous landforms (Herman et al., 2011; Sternai et al., 2013; van der Beek & Bourbon, 2008), resulting from different ice extent/thickness and erosion efficiency over glacial cycles (Pedersen & Egholm, 2013; Seguinot & Delaney, 2021). (Pedersen and Egholm, 2013; Seguinot and Delaney, 2021).

5.3 Landsliding and topographic mountain evolution

5.3.1 The glacial/interglacial transition: a hot moment for alpine erosion

Glacial erosion also does not appear to be spatially uniform throughout the glacial period (Seguinot & Delaney, 2021), and field studies have shown increased glacial erosion during the deglaciation period (M. N. Koppes & Montgomery, 2009). Therefore, hot moments of glacial dynamics occur at the end of the glacial period. Following this period, our model results suggest an additional pulse of rapid erosion, associated to landsliding, at the onset of the interglacial period. Therefore, the glacial interglacial transition seems to concentrate the most rapid rates of erosion and in turn, may participate strongly to landscape changes and topographic relief evolution in alpine settings.

However, our simulations were carried out on the current topography, which is already the results of 2 million years of successive glacial interglacial cycles. Thus, the "hot moment" of crosion that we observe in the post glacial period occurs in U shaped valleys that are already well marked. As landslide potential is maintained by steep slopes, this shape of mature glacial valley may increase landslides activity compared with early Quaternary activity and increase in the same time the key role of hillslopes processes in shaping long term mountain topography (Burbank et al., 1996; Korup et al., 2007; Larsen & Montgomery, 2012).

5.3.2 Toward a "landslide buzzsaw"?

The final landslide patterns from our simulations show interesting similarity with the morphological changes associated with the glacial buzzsaw (Fig. 6). Previous studies have highlighted the impact of glacial crosion on the mountain clevations and reliefs, referred as the 'glacial buzzsaw' (Egholm et al., 2009; Herman et al., 2013, 2021; Mitchell & Montgomery, 2006; Thomson et al., 2010; Tomkin & Braun, 2002). This theoretical concept, based on the observed correlation between the position of the Equilibrium Line Altitude (ELA) and the mean and maximum height of mountains Glacial crosion also does not appear to be spatially uniform throughout the glacial period (Seguinot and Delaney, 2021), and field studies have shown increased glacial crosion during the deglaciation period (Koppes and Montgomery, 2009). Therefore, key crosion moments of glacial dynamics occur at the end of the glacial period. Following this period, our model results suggest an additional pulse of rapid crosion, associated to landsliding within the first 10 kyr after deglaciation. Therefore, the glacial-interglacial transition seems to concentrate the most rapid rates of crosion and in turn, may contribute strongly to landscape changes and topographic relief evolution in alpine settings.

However, our simulations were carried out on the current topography, which is already the results of 2 million years of successive glacial-interglacial cycles. Thus, the hot-moment of erosion that we observe in the post-glacial period occurs in U-shaped valleys that are already well marked. As landslide potential is maintained by steep slopes, this shape of mature glacial valley may increase landslide activity compared with early Quaternary times. Overall, this reinforces the already-demonstrated key role of hillslopes processes in shaping long-term mountain topography (Burbank et al., 1996; Korup et al., 2007; Larsen and Montgomery, 2012).

5.3.2 Toward a "landslide buzzsaw"?

The final landslide patterns from our simulations show interesting similarity with the morphological changes associated with the glacial buzzsaw (Fig. 6). Previous studies have highlighted the impact of glacial erosion on mountain elevations and relief, referred as the 'glacial buzzsaw' (Egholm et al., 2009; Herman et al., 2013, 2021; Mitchell and Montgomery, 2006; Thomson et al., 2010; Tomkin and Braun, 2002). This theoretical concept, based on the observed correlation between the position of the Equilibrium Line Altitude (ELA) and the mean and maximum height of mountains (Egholm et al., 2009), suggests that glaciers may have a strong control on mountain relief. In fact, by shaping cirques, glaciers create steep slopes at high elevations (Brozović et al., 1997), increasing erosion above the ELA. Although the "glacial buzzsaw" might be more complex in specific mountain ranges (Banerjee & Wani, 2018; Scherler, 2014), a concentration of surface area is usually observed around the ELA elevation, increasing erosion above the ELA. Although the "glacial buzzsaw" might be more complex in specific mountain ranges (Banerjee and Wani, 2018; Scherler, 2014), a concentration of surface area is usually

930 observed around the ELA elevation (Egholm et al., 2009, 2017; Liebl et al., 2021; Pedersen et al., 2010; Prasicek et al., 2020; Steer et al., 2012).

For the three studied catchments, most of the landslide scars occur close to the catchment boundaries, i.e. along steep rock walls or enalong sharp ridgesridge crests of the catchments. In addition, and we observedobserve a decrease in the maximum catchment elevation and such as the glacial buzzsaw. However, we observe a concentration of hillslopes (around the angle of friction) at specific elevations over a larger elevation range (Fig. 7)-) around the shouldering than the glacial buzzsaw would be. Thus, our simulations highlight that the topographic by simulating the strong impact of landslides on slopes above the ELA seem strongly affected by landslide activity, appearing as a potential 'landslides buzzsaw'shouldering, we can question the role of hillslope erosion and similarly imagine a "landslides buzzsaw" during interglacial period-periods. Such a "landslide buzzsaw" would be more based on mechanisms presented in Mitchell and Montgomery (2006), with a perhaps more complex dependence on climate and lithology. However, by incorporating additional processes for glacial erosion, such as subglacial hydrology, the arguments underlying the glacial buzzsaw concept may also be debated regarding catchment topographic evolution (Herman et al, 2011) and become more complex. This concept of "landslide buzzsaw" may not be sustainable over long time periods since landslide activity will limit the occurrence of steep hillslopes. However, over Quaternary glacial cycles, successive glaciations and associated glacial/paraglacial erosion may sustain steep hillslopes at high elevations, further promoting the "landslide buzzsaw" during subsequent interglacial periods as proposed for instance for the European Alps (Delunel et al., 2020; Norton et al., 2010). This coupling between glacial and hillslope processes would be reinforced by the topographic impact of landsliding, affecting steep hillslopes at high elevations and producing larger lowlower slopes and lower-relief areas at or above the ELA (Fig. 6). This landscape conditioning would favor glacier development and erosion during the next glacial period, maintaining or enhancing the potential for glacial buzzsaw (Pedersen & Egholm, 2013)(Pedersen and Egholm, 2013).

956 6. Conclusions

932

933

934

935

936

937

938

939

940

941

942

943

944

945

946

947

948

949

950 |951

952 |953

954

955

957

958

959

960

961

962

963

964

965

The successive glacial-interglacial transitions during the Quaternary period have promoted landscape disequilibrium between the inherited topography and the dominant geomorphological processes. The HyLands model was used to study how post-glacial landslides shape alpine landscapes. We focused on landslide rates, locations, and the influence of interglacial processes on long-term landscape evolution.

We modeled the topographic evolution of three distinct catchments located in the Ecrins massif (French Alps, Fig.1), that we identified as glacial, intermediate glacial-fluvial and fluvial catchments based on their morphological characteristics (Fig. 2). For these three catchments, the highest and steepest slopes are the first topographic areas impacted by landslides (Fig. 6). Topographic changes are particularly pronounced in the glacial and intermediate catchments, where we observed a bimodal distribution of

landslides corresponding to the bimodal distribution of steep slopes generated by glacial erosion. In this case, the high and steep slopes are completely erasedmost rapidly modified, inducing a decrease in slopes to values that are slightly greater than the internal angle of friction (Fig. 7, 8&9). This control of hillslope processes on the maximum mountain elevations and the topographic reshaping at particular elevations leads us to propose similarities between the 'glacial buzzsaw' concept and postglacial landslideslandslide activity.

The simulation results also highlight a high frequency of landslides during the first 20 kyr of our simulations (Fig. 9&10), which is associated with higher erosion rates. Landslide activity and intensitymagnitude, and the resulting erosion rates, at the beginning of each simulation is followingfollow the morphological gradient (from glacial to fluvial) observed in our three catchments (Fig.11). Therefore, glacial topographic inheritance induces an intense period of post-glacial landslide activity, leading in turn possibly to regular 'hot-moments' of landscape dynamics over the Quaternary.

Our study also concludes that <a href="https://hittps://h

Finally, this study provides a basic but sound-model for understanding landslide dynamics and their impact on alpine landscape evolution. Additional components could be incorporated to enhance the model, such as fluvial processes, permafrost degradation or non-uniform rock properties to better capture the complex interactions occurring in mountain environmentenvironments. In a future work, we intend to model the interactions between hillslope processes and glacial processes over multiple glacial-interglacial cycles to better estimate their relative contributions.

|974

Author contributions. CA conducted the model calibration and analysis with support from BC. CA, PS and PV conceived the study and developed the methodology. All the authors were involved in writing and reviewing the paper.

993 Competing interests. The contact author has declared that neither they nor their co-authors have any994 competing interests.

Acknowledgements. The authors would like to thanks helpers who make this study easier, especially Diego Cusicanqui for the lidar extraction tool (https://doi.org/10.5281/zenodo.13832516) and Xavier

997 Robert for his help in adapting the simple-swath Python tool

(https://doi.org/10.5281/zenodo.13771754). Thanks to Boris Gailleton for his advice on coding and to

Field Code Changed

Field Code Changed

999	Dimitri Lague for his insightful comments on landslide dynamicsThe authors would like to thank the	
1000	two reviewers for their detailed proofreading and very constructive comments.	
1001	Financial support. This research has been supported by the H2020 European Research Council (grant	
1002	no. 803721). PGV acknowledges support from the French ANR-PIA programme (ANR-18-MPGA-	
1003	0006). BC acknowledges support from the Dutch Research Council (NWO) under the grant	
1004	OCENW.M.23.027.	
1005	References	
1006	Anderson, R. S., Molnar, P., ∧ Kessler, M. A. (2006): Features of glacial valley profiles simply	
1007	explained., Journal of Geophysical Research: Earth Surface, 111(F1).	Formatted: Font: Not Italic
1008	https://doi.org/10.1029/2005JF000344 <u>, 2006.</u>	Formatted: Font: Not Italic
1000	Antonione C. O. and Lene C. N. (2024). Codiment right consolidation Account of model	Torridated Forte Not Italie
1009 1010	Antoniazza, G., & and Lane, S. N. (2021).: Sediment yield over glacial cycles: A conceptual model. Progress in Physical Geography, 45(6), 842–865, https://doi.org/10.1177/0309133321997292,	Formatted: Font: Not Italic
1011	2021.	Formatted: Font: Not Italic
1012	D. H. J. C. W. (2002) D. J. J. J. J. D. J. C. J. D. J. 20/40) A J.	
1012 1013	Ballantyne, C. K . (2002). Paraglacial geomorphology. Quaternary Science Reviews, 21(18), Article 18-, 1935–2017, https://doi.org/10.1016/S0277-3791(02)00005-7, 2002.	Formatted: Font: Not Italic
1013	10.,1333 2017, https://doi.org/10.1010/3017/10731(02)00003 7,2001.	Formatted: Font: Not Italic
1014	Banerjee, A., &. and Wani, B. A. (2018) Exponentially decreasing erosion rates protect the high-	
1015 1016	elevation crests of the Himalaya _{T₂} <u>Earth and Planetary Science Letters</u> , <u>497</u> , 22—28-,	Formatted: Font: Not Italic
1016	https://doi.org/10.1016/j.epsl.2018.06.001 <u>, 2018.</u>	Formatted: Font: Not Italic
1017	Barféty, J. C., Pécher, A., Bambrier, A., Demeulemeester, P., Fourneaux, J. C., Poulain, P. A., Vernet, J.,	
1018	∧ Vivier, G. (1984) Notice explicative de la feuille Saint-Christophe-en-Oisans à 1/50000-,	
1019	Bureau de Recherches Géologiques et Minière: Orléans <u>, 1984</u> .	Formatted: Font: Not Italic
1020	Barnhart, K. R., Hutton, E. W. H., Tucker, G. E., Gasparini, N. M., Istanbulluoglu, E., Hobley, D. E. J.,	Formatted: English (United States)
1021	Lyons, N. J., Mouchene, M., Nudurupati, S. S., Adams, J. M., ∧ Bandaragoda, C. (2020); Short	Formatted: English (United States)
1022 1023	communication :: Landlab v2.0: a software package for Earth surface dynamics, <u>Earth Surface</u> Dynamics, <u>8(2)</u> , 379—397, https://doi.org/10.5194/esurf-8-379-2020, <u>2020.</u>	Formatted: English (United States)
1023	5/10/11/05/5/ <u>5/2-1/1</u> 5/3 _55/1/10/15/6/10/5/5/5/5/5/5/5/5/5/5/5/5/5/5/5/5/5/5/	Formatted: Font: Not Italic
1024	van der Beek, P. and Bourbon, P.: A quantification of the glacial imprint on relief development in the	Formatted: Font: Not Italic
1025 1026	French western Alps, Geomorphology, 97, 52–72, https://doi.org/10.1016/j.geomorph.2007.02.038, 2008.	
1020	2006.	
1027	Bennett, G. I., Molnar, P., Eisenbeiss, H., & McArdell, B. w. (2012) Erosional power in the Swiss	
1028	Alps: Characterization: characterization of slope failure in the Illgraben-, Earth Surface Processes and	Formatted: Font: Not Italic
1029	Landforms, 37 (15), 1627—1640-, https://doi.org/10.1002/esp.3263, 2012.	Formatted: Font: Not Italic
1030	Bernard, M., van der Beek, P. A., Pedersen, V. K., and Colleps, C.: Production and Preservation of	
1031	Elevated Low-Relief Surfaces in Mountainous Landscapes by Pliocene-Quaternary Glaciations, AGU	
1032	Advances, 6, e2024AV001610, https://doi.org/10.1029/2024AV001610, 2025.	
1033	von Blanckenburg, F.: The control mechanisms of erosion and weathering at basin scale from	
1034	cosmogenic nuclides in river sediment, Earth and Planetary Science Letters, 237, 462–479,	
1035	https://doi.org/10.1016/j.epsl.2005.06.030, 2005.	
1		

1036	Blondeau, S., Gunnell, Y., ∧ Jarman, D. (2021) Rock slope failure in the Western Alps-:: A first		
1037	comprehensive inventory and spatial analysis- ₁ , Geomorphology, 380, 107622- ₂		Formatted: Font: Not Italic
1038	https://doi.org/10.1016/j.geomorph.2021.107622 <u>, 2021.</u>		Formatted: Font: Not Italic
1039	Brardinoni, F., & and Hassan, M. A. (2007) Glacially induced organization of channel-reach	,	
1040	morphology in mountain streams. Journal of Geophysical Research: Earth Surface, 112(F3).		Formatted: Font: Not Italic
1041	https://doi.org/10.1029/2006JF000741 <u>, 2007.</u>		Formatted: Font: Not Italic
1042	Brocklehurst, S. H., &. and Whipple, K. X. (2006) Assessing the relative efficiency of fluvial and	(
1042	glacial erosion through simulation of fluvial landscapes, Geomorphology, 75(3), 283–299,		Formatted: Font: Not Italic
1044	https://doi.org/10.1016/j.geomorph.2005.07.028, 2006.		Formatted: Font: Not Italic
10.45	Durandari I. Dansi M. Liiman V. Camurfanta D. Dansan I. Sand Vannasandra M. (2020) . Landalida		Tomatea. Fort. Not have
1045 1046	Broeckx, J., Rossi, M., Lijnen, K., Campforts, B., Poesen, J., <u>∧</u> Vanmaercke, M . (2020). Landslide mobilization rates ∴ A global analysis and model LEarth-Science Reviews, 201, 102972.		Formatted: Font: Not Italic
1047	https://doi.org/10.1016/j.earscirev.2019.102972 <u>, 2020.</u>	\leq	Formatted: Font: Not Italic
		l	Formatted. Fort. Not Italic
1 048 1049	Brown, E. T., Stallard, R. F., Larsen, M. C., Raisbeck, G. M., & and Yiou, F. (1995) Denudation rates determined from the accumulation of in situ-produced 10Be in the luquillo experimental forest,		
1050	Puerto Rico _{7, E} arth and Planetary Science Letters, 129(1), 193–202, https://doi.org/10.1016/0012-		Formatted: Font: Not Italic
1051	821X(94)00249-X <u>, 1995.</u>		Formatted: Font: Not Italic
1052	Brozović, N., Burbank, D. W., ∧ Meigs, A. J . (1997) Climatic Limits on Landscape Development in	(
1052	the Northwestern Himalaya-, Science, 276 (5312), 571–574-,		Formatted: Font: Not Italic
1054	https://doi.org/10.1126/science.276.5312.571, 1997.	\leq	Formatted: Font: Not Italic
4055		l	Tomatted. Fort. Not Italic
1055 1056	Buechi, M. W., Graf, H. R., Haldimann, P., Lowick, S. E., <u>∧</u> Anselmetti, F. S . (2018). Multiple Quaternary erosion and infill cycles in overdeepened basins of the northern Alpine foreland. Swiss	_	Formatted: Font: Not Italic
1057	Journal of Geosciences J Geosci, 111(1), Article 1., 133–167, https://doi.org/10.1007/s00015-017-		
1058	0289-9 <u>, 2018.</u>		Formatted: Font: Not Italic
1059	Burbank, D. W., Leland, J., Fielding, E., Anderson, R. S., Brozovic, N., Reid, M. R., ∧ Duncan, C-		
1060	(1996).: Bedrock incision, rock uplift and threshold hillslopes in the northwestern Himalayas.		
1061	Nature, 379 (6565), 505510-, https://doi.org/10.1038/379505a0, 1996.		Formatted: Font: Not Italic
1062	Campforts, B., Shobe, C. M., Overeem, I., & Tucker, G. E. (2022). The Art of Landslides : How	1	Formatted: Font: Not Italic
1063	Stochastic Mass Wasting Shapes Topography and Influences Landscape Dynamics. Journal of		
1064	Geophysical Research: Earth Surface, 127(8), e2022JF006745. https://doi.org/10.1029/2022JF006745		
1065	Campforts B. Shoho C. M. Stoor B. Vanmaorsko M. Lague D. Rand Braun J. (2020) ellistanda		
1065 1066	Campforts, B., Shobe, C. M., Steer, P., Vanmaercke, M., Lague, D., & Braun, J. (2020) HyLands 1.0:-A: a hybrid landscape evolution model to simulate the impact of landslides and landslide-		
1067	derived sediment on landscape evolution-, Geoscientific Model Development, 13(9), 3863—3886-,		Formatted: Font: Not Italic
1068	https://doi.org/10.5194/gmd-13-3863-2020 <u>, 2020.</u>		Formatted: Font: Not Italic
1069	Campforts, B., Shobe, C. M., Overeem, I., and Tucker, G. E.: The Art of Landslides: How Stochastic		
1070	Mass Wasting Shapes Topography and Influences Landscape Dynamics, Journal of Geophysical		
1071	Research: Earth Surface, 127, e2022JF006745, https://doi.org/10.1029/2022JF006745, 2022.		
1072	Carretier, S., Martinod, P., Reich, M., ∧ Godderis, Y . (2016). .: Modelling sediment clasts transport		
1072	during landscape evolution ₇ , Farth Surface Dynamics, 4(1), 237-251-, https://doi.org/10.5194/esurf-		Formatted: Font: Not Italic
1074	4-237-2016 <u>, 2016.</u>	Y	Formatted: Font: Not Italic
1075	Carriere, A., Le Bouteiller, C., Tucker, G. E., Klotz, S., & Naaim, M. (2020) Impact of vegetation		
1075	on erosion -: Insights from the calibration and test of a landscape evolution model in alpine badland		
'			

1077	catchments-, Earth Surface Processes and Landforms, 45(5), 10851099-,	Formatted	[1]
1078	https://doi.org/10.1002/esp.4741 <u>, 2020.</u>	Formatted	[2]
4070		Formatted	[3]
1079	Cathala, M., Magnin, F., Ravanel, L., Dorren, L., Zuanon, N., Berger, F., Bourrier, F., ∧ Deline, P.	Formatted	[4]
1080 1081	(2024) Mapping release and propagation areas of permafrost-related rock slope failures in the French Alps-: A new methodological approach at regional scale Geomorphology, 448, 109032	Formatted	[5]
1082	https://doi.org/10.1016/j.geomorph.2023.109032, 2024.	Formatted	[6]
	//	Formatted	
1083	Cavalli, M., Heckmann, T., & and Marchi, L. (2019) Sediment Connectivity in Proglacial Areas. In T.	Formatted	[7]
1084	Heckmann & D. Morche (Éds.), in: Geomorphology of Proglacial Systems :: Landform and Sediment	//>	[8]
1085 1086	Dynamics in Recently Deglaciated Alpine Landscapes (p. 271-287)., edited by: Heckmann, T. and Morche, D., Springer International Publishing-, Cham, 271–287, https://doi.org/10.1007/978-3-319-	Formatted	[9]
1087	94184-4_16, 2019.	Formatted	[[10]
		Formatted	[11]
1088	Champagnac, JD., Valla, P. G., & and Herman, F. (2014): Late-Cenozoic relief evolution under	Formatted	[12]
1089	evolving climate-: A review-, Tectonophysics, 614, 4465-,	Formatted	[13]
1090	https://doi.org/10.1016/j.tecto.2013.11.037 <u>, 2014.</u>	Formatted	[14]
1091	Claessens, L., Schoorl, J. M., & Veldkamp, A. (2007) Modelling the location of shallow landslides	Formatted	([15]
1092	and their effects on landscape dynamics in large watersheds÷: An application for Northern New	Formatted	[16]
1093	Zealand ₋₁ , Geomorphology, 87 (1), 16- <u>-</u> 27 ₋₁ https://doi.org/10.1016/j.geomorph.2006.06.039, <u>2007.</u>	Formatted	
1004	Consisti F. Adro J. Donne D. Dell'Armone A. Frank Ad. Dethburn C. Sand Couplli Ad. (2010)		[17]
1094 1095	Comiti, F., Mao, L., Penna, D., Dell'Agnese, A., Engel, M., Rathburn, S., & and Cavalli, M. (2019) Glacier melt runoff controls bedload transport in Alpine catchments. Earth and Planetary Science	Formatted	[18]
1096	Letters, 520, 77—86-, https://doi.org/10.1016/j.epsl.2019.05.031, 2019.	Formatted	[19]
	, , , , , , , , , , , , , , , , , , ,	Formatted	[20]
1097	Cossart, É . (2013). : Influence of local vs. Regional regional settings on glaciation patterns in the	Formatted	[21]
1098	French Alps-, Geografia Fisica e Dinamica Quaternaria, 36 (1), Article 1., 39–52 ,	Formatted	[22]
1099	https://doi.org/10.4461/GFDQ.2013.36.3 <u>, 2013</u>	Formatted	[23]
1100	Cossart, E., Braucher, R., Fort, M., Bourlès, D. L., & Carcaillet, J. (2008) Slope instability in	Formatted	[[24]
1101	relation to glacial debuttressing in alpine areas (Upper Durance catchment, southeastern France):	Formatted	[25]
1102	Evidence from field data and 10Be cosmic ray exposure ages ₋₁ , Geomorphology, 95(1), 3-26-4	Formatted	
1103	https://doi.org/10.1016/j.geomorph.2006.12.022 <u>, 2008.</u>	Formatted	[26]
1104	Coutterand, S . (2010) Étude géomophologique des flux glaciaires dans les Alpes nord-occidentales		[27]
1105	au Pléistocène récent. Du maximum de la dernière glaciation aux premières étapes de la déglaciation	Formatted	[28]
1106	[Phdthesis, phdthesis, Université de Savoie]. https://theses.hal.science/tel-00517790, 2010.	Formatted	[[29]]
		Formatted	[30]
1107	Croissant, T., Lague, D., Steer, P., ∧ Davy, P. (2017) Rapid post-seismic landslide evacuation	Formatted	[31]
1108 1109	boosted by dynamic river width, Nature GeoscienceGeosci, 10 (9), Article 9., 680–684, https://doi.org/10.1038/ngeo3005, 2017.	Formatted	[32]
1.03	11049-17 4011016 2012030 118003003 <u>, 2017 1</u>	Formatted	[[33]
1110	Culmann, K . (avec University of Michigan). (1875) Die graphische Statik. Zürich, Meyer & Zeller (A.	Formatted	[[34]
1111	Reimann). http://archive.org/details/diegraphischest01culmgoog), 744 pp., 1875.	Formatted	
1112	Cusicangui, D. (2024) cusicand/lidarhd ign downloader : V3.0 (Version: v3.0) [Logiciel]. Zenodo.,	Formatted	[35]
1112	https://doi.org/10.5281/zenodo.13832516, 2024.	/ \	[[36]
1		Formatted	[37]
1114	Dahlquist, M. P., West, A. J., & and Li, G. (2018) Landslide-driven drainage divide migration.	Formatted	[[38]
1115	Geology, 46 (5), Article 5., 403–406, https://doi.org/10.1130/G39916.1, 2018.	Formatted	[39]
I		Formatted	[40]
		Formatted	[41]

Formatted

... [41]

1116	Davy, P., Croissant, T., & and Lague, D. (2017) A precipiton method to calculate river		Formatted: English (United States)
1117	hydrodynamics, with applications to flood prediction, landscape evolution models, and braiding	<	
1118	instabilities: Journal of Geophysical Research: Earth Surface, 122(8), 1491—1512:		Formatted: English (United States)
1119	https://doi.org/10.1002/2016JF004156 <u>, 2017.</u>		Formatted: Font: Not Italic
1120	Delayde F. Zenethe C. Calcurate C. Mathieur D. Gand Demography C. (2022). Househors of laws		Formatted: Font: Not Italic
1120 1121	Delgado, F., Zerathe, S., Schwartz, S., Mathieux, B., & and Benavente, C. (2022) Inventory of large		
1121	landslides along the Central Western Andes (ca. 15°–20° S)-:): Landslide distribution patterns and insights on controlling factors, Journal of South American Earth Sciences, 116, 103824,	_	Farmanttade Faret Nat Halia
1123	https://doi.org/10.1016/j.jsames.2022.103824, 2022.	<	Formatted: Font: Not Italic
1123	11(tp3.//doi.o1g/10.1010/j.j.dui103.2022.103024 <u>, 2022.</u>		Formatted: Font: Not Italic
1124	Delunel, R., van der Beek, P. A., Carcaillet, J., Bourlès, D. L., and Valla, P. G.: Frost-cracking control on		
1125	catchment denudation rates: Insights from in situ produced 10Be concentrations in stream		
1126	sediments (Ecrins–Pelvoux massif, French Western Alps), Earth and Planetary Science Letters, 293,		
1127	72–83, https://doi.org/10.1016/j.epsl.2010.02.020, 2010.		
1128	Delunel, R., van der Beek, P. A., Bourlès, D. L., Carcaillet, J., and Schlunegger, F.: Transient sediment		
1129	supply in a high-altitude Alpine environment evidenced through a 10Be budget of the Etages		
1130	catchment (French Western Alps), Earth Surface Processes and Landforms, 39, 890–899,		
1131	https://doi.org/10.1002/esp.3494, 2014.		
1132	Delunel, R., Schlunegger, F., Valla, P. G., Dixon, J., Glotzbach, C., Hippe, K., Kober, F., Molliex, S.,		
1133	Norton, K. P., Salcher, B., Wittmann, H., Akçar, N., & Christl, M . (2020). Late-Pleistocene		
1134	catchment-wide denudation patterns across the European Alps _z , <u>Earth-Science Reviews</u> , <u>211</u> ,		Formatted: Font: Not Italic
1135	103407- _{z.} https://doi.org/10.1016/j.earscirev.2020.103407 <u>. 2020.</u>		Formatted: Font: Not Italic
1136	Delunel, R., van der Beek, P. A., Bourlès, D. L., Carcaillet, J., & Schlunegger, F. (2014). Transient		
1137	sediment supply in a high-altitude Alpine environment evidenced through a 10Be budget of the		
1138	Etages catchment (French Western Alps). Earth Surface Processes and Landforms, 39(7), 890-899.		
1139	https://doi.org/10.1002/esp.3494		
11.40	Delivery D. Correllet D. A. Correllet I. Dovid's D. L. O. Vella, D. C. (2010). For expension		
1140 1141	Delunel, R., van der Beek, P. A., Carcaillet, J., Bourlès, D. L., & Valla, P. G. (2010). Frost-cracking control on catchment denudation rates: Insights from in situ produced 10Be concentrations in		
1141	stream sediments (Ecrins-Pelvoux massif, French Western Alps). Earth and Planetary Science Letters,		
1143	293(1), 72-83. https://doi.org/10.1016/j.epsl.2010.02.020		
	to the state of th		
1144	Densmore, A. L., Ellis, M. A., & and Anderson, R. S. (1998): Landsliding and the evolution of normal-		
1145	fault-bounded mountains-, Journal of Geophysical Research: Solid Earth, 103(87), 15203-15219-		Formatted: Font: Not Italic
1146	https://doi.org/10.1029/98JB00510 <u>, 1998.</u>		Formatted: Font: Not Italic
1147	Dietrich, W. E., Reiss, R., Hsu, ML., ∧ Montgomery, D. R. (1995) A process-based model for		
1148	colluvial soil depth and shallow landsliding using digital elevation data-, Hydrological Processes,		Formatted: Font: Not Italic
1149	9 (3-4), 383–400-, https://doi.org/10.1002/hyp.3360090311, 1995.		
			Formatted: Font: Not Italic
1150	Egholm, D. L., Nielsen, S. B., Pedersen, V. K., and Lesemann, JE.: Glacial effects limiting mountain		
1151	height, Nature, 460, 884–887, https://doi.org/10.1038/nature08263, 2009.		
1152	Egholm, D. L., Jansen, J. D., Brædstrup, C. F., Pedersen, V. K., Andersen, J. L., Ugelvig, S. V., Larsen, N.		
1153	K., & K., and Knudsen, M. F. (2017): Formation of plateau landscapes on glaciated continental margins.		
1154	Nature <u>GeoscienceGeosci</u> , 10 (8), 592–597-, https://doi.org/10.1038/ngeo2980, <u>2017.</u>		Formatted: Font: Not Italic
			Formatted: Font: Not Italic
1155	Egholm, D. L., Nielsen, S. B., Pedersen, V. K., & Lesemann, J. E. (2009). Glacial effects limiting		Torridated. Fort. Not italic
1156	mountain height. Nature, 460(7257), 884-887. https://doi.org/10.1038/nature08263		

1157 1158	Fox, M., Herman, F., Kissling, E., & Willett, S. D. (2015). Rapid exhumation in the Western Alps driven by slab detachment and glacial erosion. <i>Geology</i> , 43(5), 379–382. https://doi.org/10.1130/G36411.1	
1159	French, H. M . (2017) The Periglacial Environment, John Wiley & Sons, 565 pp., 2017 .	Formatted: Font: Not Italic
1160 1161	Gallach, X., Carcaillet, J., Ravanel, L., Deline, P., Ogier, C., Rossi, M., Malet, E., & and Garcia-Sellés, D-(2020) Climatic and structural controls on Late-glacial and Holocene rockfall occurrence in high-	
1162	elevated rock walls of the Mont Blanc massif (Western Alps-), Earth Surface Processes and	Formatted: Font: Not Italic
1163	Landforms, 45 (13), 3071—3091-, https://doi.org/10.1002/esp.4952 <u>, 2020.</u>	Formatted: Font: Not Italic
1164	Ganti, V., von-Hagke, C., Scherler, D., Lamb, M. P., Fischer, W. W., & Avouac, JP. (2016) Time	
1165	scale bias in erosion rates of glaciated landscapes- _{2.} Science Advances, 2 (10), Article 10. , e1600204,	Formatted: Font: Not Italic
1166	https://doi.org/10.1126/sciadv.1600204 <u>, 2016.</u>	Formatted: Font: Not Italic
1167	George, D. L., & and Iverson, R. M. (2014) A depth-averaged debris-flow model that includes the	
1168	effects of evolving dilatancy. II. Numerical predictions and experimental tests ₁ , Proceedings of the	Formatted: Font: Not Italic
1169	Royal Society A: Mathematical, Physical and Engineering Sciences, 470 (2170), 20130820-	Formatted: Font: Not Italic
1170	https://doi.org/10.1098/rspa.2013.0820 <u>, 2014.</u>	
1171	Guzzetti, F., Malamud, B. D., Turcotte, D. L., & Reichenbach, P. (2002) Power-law correlations of	
1172	landslide areas in central Italy-, Earth and Planetary Science Letters, 195 (3), 169-–183-,	Formatted: Font: Not Italic
1173	https://doi.org/10.1016/S0012-821X(01)00589-1 <u>, 2002.</u>	Formatted: Font: Not Italic
1174	Hallet, B., Hunter, L., & Bogen, J. (1996) Rates of erosion and sediment evacuation by glaciers:	
1175	A review of field data and their implications _{-z} Global and Planetary Change, 12(1), Article 1., 213–235,	Formatted: Font: Not Italic
1176	https://doi.org/10.1016/0921-8181(95)00021-6 <u>, 1996.</u>	Formatted: Font: Not Italic
1177	Heimsath, A. M., Furbish, D. J., ∧ Dietrich, W. E . (2005) The illusion of diffusion ÷: Field evidence	
1178	for depth-dependent sediment transport., Geology, 33(12), 949–952.	Formatted: Font: Not Italic
1179	https://doi.org/10.1130/G21868.1 <u>, 2005.</u>	Formatted: Font: Not Italic
1180	Hergarten, S., &. and Robl, J. (2015): Modelling rapid mass movements using the shallow water	
1181	equations in Cartesian coordinates., Natural Hazards and Earth System Sciences, 15(3), 671—685.	Formatted: Font: Not Italic
1182	https://doi.org/10.5194/nhess-15-671-2015 <u>, 2015.</u>	Formatted: Font: Not Italic
1183	Herman, F. and Herman, F., Beaud, F., Champagnac, JD., Lemieux, JM., & Sternai, P. (2011). Glacial	
1184	hydrology and erosion patterns: A mechanism for carving glacial valleys. Earth and Planetary Science	Formatted: English (United States)
1185	Letters, 310(3), 498-508. https://doi.org/10.1016/j.epsl.2011.08.022	Formatted: Font: Not Italic
		Formatted: Font: Not Italic
1186	Herman, F., & Braun, J. (2008) Evolution of the glacial landscape of the Southern Alps of New	Formatted: English (United States)
1187 1188	Zealand : Insights from a glacial erosion model . Journal of Geophysical Research: Earth Surface, 113(F2). https://doi.org/10.1029/2007JF000807, 2008.	Formatted: English (United States)
		Formatted: English (United States)
1189	Herman, F., & and Champagnac, JD. (2016) Plio-Pleistocene increase of erosion rates in mountain	Formatted: Font: Not Italic, English (United States)
1190 1191	belts in response to climate change-, Terra Nova, 28(1), 2-10-, https://doi.org/10.1111/ter.12186, 2016.	Formatted: English (United States)
1131	2010,	Formatted: Font: Not Italic, English (United States)
1192	Herman, F., Beaud, F., Champagnac, JD., Lemieux, JM., Herman, F., De Doncker, F., Delaney, I.,	Formatted: English (United States)
1193 1194	Prasicek, G., & Koppes, M. (2021). The impact of glaciers on mountainand Sternai, P.: Glacial hydrology and erosion. Natura Payiews patterns: A mechanism for caping glacial valleys. Earth &	Formatted: English (United States)
1194 1195	hydrology and erosion. Nature Reviews patterns: A mechanism for carving glacial valleys, Earth & Environment, 2(6), 422-435, and Planetary Science Letters, 310, 498–508,	Formatted: English (United States)
1196	https://doi.org/10.1 038/s43017-021-00165-9 1016/j.epsl.2011.08.022, 2011.	Formatted: English (United States)
		Formatted: Font: Not Italic
		Tornatteu. Fort. Not Italic

1197	Herman, F., Seward, D., Valla, P. G., Carter, A., Kohn, B., Willett, S. D., & and Ehlers, T. A. (2013)	
1198	Worldwide acceleration of mountain erosion under a cooling climate ₋ Nature, 504(7480), 423—	Formatted: Font: Not Italic
1199	426-, https://doi.org/10.1038/nature12877, 2013.	Formatted: Font: Not Italic
1200	Herman, F., De Doncker, F., Delaney, I., Prasicek, G., and Koppes, M.: The impact of glaciers on	
1200	mountain erosion, Nat Rev Earth Environ, 2, 422–435, https://doi.org/10.1038/s43017-021-00165-9,	
1202	2021.	
1202	2021.	
1203	Hobley, D. E. J., Adams, J. M., Nudurupati, S. S., Hutton, E. W. H., Gasparini, N. M., Istanbulluoglu, E.,	
1204	∧ Tucker, G. E. (2017) Creative computing with Landlab : An: an open-source toolkit for	
1205	building, coupling, and exploring two-dimensional numerical models of Earth-surface dynamics-	
1206	Earth Surface Dynamics, 5(1), 21-46, https://doi.org/10.5194/esurf-5-21-2017, 2017.	Formatted: Font: Not Italic
1207	Hooke, J . (2003) : Coarse sediment connectivity in river channel systems : A: a conceptual framework	Formatted: Font: Not Italic
1207	and methodology-, Geomorphology, 56(1), Article 1., 79–94, https://doi.org/10.1016/S0169-	Formatted: Font: Not Italic
1209	555X(03)00047-3, <u>2003.</u>	
	· , — —	Formatted: Font: Not Italic
1210	Hovius, N., Stark, C. P., ∧ Allen, P. A. (1997) Sediment flux from a mountain belt derived by	
1211	landslide mapping- <u>,</u> Geology, 25 (3), 231- <u>-</u> 234- <u>,</u> https://doi.org/10.1130/0091-	Formatted: Font: Not Italic
1212	7613(1997)025<0231:SFFAMB>2.3.CO;2 <u>, 1997.</u>	Formatted: Font: Not Italic
1213	Hovius, N., Stark, C. P., Hao-Tsu, C., & Jiun-Chuan, L. (2000) Supply and Removal of Sediment in	
1214	a Landslide-Dominated Mountain Belt :: Central Range, Taiwan , The Journal of Geology, 108(1), 73-	Formatted: Font: Not Italic
1215	89-, https://doi.org/10.1086/314387, 2000.	Formatted: Font: Not Italic
		Formatteu. Forth. Not Italic
1216	Ivy-Ochs, S., Martin, S., Campedel, P., Hippe, K., Alfimov, V., Vockenhuber, C., Andreotti, E., Carugati,	
1217	G., Pasqual, D., Rigo, M., ∧ Viganò, A. (2017) Geomorphology and age of the Marocche di Dro	
1218 1219	rock avalanches (Trentino, Italy)-, Quaternary Science Reviews, 169, 188—205-,	Formatted: Font: Not Italic
1219	https://doi.org/10.1016/j.quascirev.2017.05.014 <u>, 2017.</u>	Formatted: Font: Not Italic
1220	Jeandet, L., Steer, P., Lague, D., & Davy, P. (2019). Coulomb Mechanics and Relief Constraints Explain	Formatted: Font: Not Italic
1221	Landslide Size Distribution—_Jeandet—_2019—_Geophysical Research Letters—_Wiley Online	Formatted: Font: Not Italic
1222 1223	Library- <u>:</u> https://agupubs.onlinelibrary.wiley.com/doi/full/10.1029/2019GL082351, last access: 21 September 2023.	Formatted: Font: Not Italic
1223	September 2023.	Formatted: Font: Not Italic
1224	Keefer, D. K . (1984) Landslides caused by earthquakes-, GSA Bulletin, 95(4), 406-421-	Formatted: Font: Not Italic
1225	https://doi.org/10.1130/0016-7606(1984)95<406:LCBE>2.0.CO;2 <u>, 1984.</u>	Formatted: Font: Not Italic
1226	Koppes, M., Hallet, B., Rignot, E., Mouginot, J., Wellner, J. S., ∧ Boldt, K. (2015): Observed	Formatted: Font: Not Italic
1227	latitudinal variations in erosion as a function of glacier dynamics. Nature, 526(7571), 100-103-1	Formatted: Font: Not Italic
1228	https://doi.org/10.1038/nature15385 <u>, 2015.</u>	
		Formatted: Font: Not Italic
1229	Koppes, M. N., & and Montgomery, D. R. (2009) The relative efficacy of fluvial and glacial erosion	
1230 1231	over modern to orogenic timescales- _{1.} Nature GeoscienceGeosci, 2(9), 644-647- https://doi.org/10.1038/ngeo616, 2009.	Formatted: Font: Not Italic
1231	https://doi.org/10.1036/fige0010 <u>, 2003.</u>	Formatted: Font: Not Italic
1232	Korup, O. (2006): Effects of large deep-seated landslides on hillslope morphology, western Southern	
1233	Alps, New Zealand-, Journal of Geophysical Research: Earth Surface, 111 (F1), Article F1.	Formatted: Font: Not Italic
1234	https://doi.org/10.1029/2004JF000242 <u>, 2006.</u>	Formatted: Font: Not Italic
1235	Korup, O., Clague, J. J., Hermanns, R. L., Hewitt, K., Strom, A. L., & Weidinger, J. T. (2007) Giant	
1236	landslides, topography, and erosion-, Earth and Planetary Science Letters, 261(3), 578—589-,	Formatted: Font: Not Italic
1237	https://doi.org/10.1016/j.epsl.2007.07.025 <u>, 2007.</u>	Formatted: Font: Not Italic

1238	Kuhlemann, J., Frisch, W., Székely, B., Dunkl, I., & Kázmér, M. (2002).: Post-collisional sediment		
1239	budget history of the Alps : Tectonic: tectonic versus climatic control. International Journal of, Int J.		Formatted: Font: Not Italic
1240	Earth Sciences, Sci (Geol Rundsch), 91(5), 818–837. https://doi.org/10.1007/s00531-002-0266-y		Formatted: Font; Not Italic
1241	2002.		romatteu. Fort. Not italic
1242	Lane, S. N., Bakker, M., Gabbud, C., Micheletti, N., & Sand Saugy, JN. (2017) Sediment export,		
1243	transient landscape response and catchment-scale connectivity following rapid climate warming and		
1244	Alpine glacier recession-, Geomorphology, 277, 210-–227-,		Formatted: Font: Not Italic
1245	https://doi.org/10.1016/j.geomorph.2016.02.015 <u>, 2017.</u>		Formatted: Font: Not Italic
1246	Langeton, A. L. 9, and Tucker, C. F. (2010). Developing and evaluring a theory for the lateral		13 martea : ond : roc italic
1240	Langston, A. L., & and Tucker, G. E. (2018).: Developing and exploring a theory for the lateral erosion of bedrock channels for use in landscape evolution models., Earth Surface Dynamics, 6(, 1),		Francis d Francis North Pr
1248	Article 1.—27, https://doi.org/10.5194/esurf-6-1-2018, 2018.	<	Formatted: Font: Not Italic
1240	Price 1: 27, https://doi.org/10.3134/esun-0-1-2010, 2010.		Formatted: Font: Not Italic
1249	Larsen, I. J ., & and Montgomery, D. R . (2012) Landslide erosion coupled to tectonics and river		
1250	incision _{-L.} Nature Geoscience Geosci, 5(7), 468-473-, https://doi.org/10.1038/ngeo1479, 2012.		Formatted: Font: Not Italic, English (United States)
1251	Lavé, J., Guérin, C., Valla, P. G., Guillou, V., Rigaudier, T., Benedetti, L., France-Lanord, C., Gajurel, A.		Formatted: English (United States)
1251	P., Morin, G., Dumoulin, J. P., Moreau, C., & And Galy, V. (2023) Medieval demise of a Himalayan		Formatted: Font: Not Italic, English (United States)
1253	giant summit induced by mega-landslide-, Nature, 619(7968), 94–101-,	, ///	Formatted: English (United States)
1254	https://doi.org/10.1038/s41586-023-06040-5 <u>, 2023.</u>	// //	Formatted: English (United States)
1255	La Roy M. Dalina D. Carsaillat I. Schimmalafannia I. Sand Ermini M. (2017) (100a aynasura		Formatted: English (United States)
1 255 1256	Le Roy, M., Deline, P., Carcaillet, J., Schimmelpfennig, I., & and Ermini, M. (2017) 10Be exposure dating of the timing of Neoglacial glacier advances in the Ecrins-Pelvoux massif, southern French		Formatted: English (United States)
1257	Alps-, Quaternary Science Reviews, 178, 118–138-, https://doi.org/10.1016/j.quascirev.2017.10.010,	- ///	\
1258	2017.	\ \\	Formatted: English (United States)
		1 1	Formatted: English (United States)
1259 1260	Lebrouc, V., Schwartz, S., Baillet, L., Jongmans, D., ∧ Gamond, J. F. (2013) Modeling permafrost	_ // `	Formatted: Font: Not Italic
1261	extension in a rock slope since the Last Glacial Maximum-: Application to the large Séchilienne landslide (French Alps)-], Geomorphology, 198, 189–200-,	//	Formatted: Font: Not Italic
1262	https://doi.org/10.1016/j.geomorph.2013.06.001 <u>, 2013.</u>	/ /	Formatted: Font: Not Italic
			Formatted: Font: Not Italic
1263	Lehmann, B., & and Robert, X. (2024). Simple: simple swath, a simple Python code to extract swath	, /	Formatted: Font: Not Italic
1264 1265	profile using a shapefile (Version 2.0.0) [Logiciel]. Zenodo., https://doi.org/10.5281/zenodo.13771754, 2024.		Formatted: Font: Not Italic
1205	https://doi.org/10.5281/2eHodo.15771754 <u>, 2024.</u>		Formatted: Font: Not Italic
1266	Leith, K., Fox, M., & Moore, J. R. (2018). Signatures of Late Pleistocene fluvial incision in an Alpine		
1267	landscape. Earth and Planetary Science Letters, 483, 13-28.		
1268	https://doi.org/10.1016/j.epsl.2017.11.050		
1269	Leith, K., Moore, J. R., Amann, F., & Loew, S. (2014) Subglacial extensional fracture		
1270	development and implications for Alpine Valley evolution, Journal of Geophysical Research: Earth		Formatted: Font: Not Italic
1271	Surface, 119 (1), 62–81-, https://doi.org/10.1002/2012JF002691, 2014.		Formatted: Font: Not Italic
4070			Torridated. Fort. Not realic
1272 1273	<u>Leith, K., Fox, M., and Moore, J. R.: Signatures of Late Pleistocene fluvial incision in an Alpine</u> landscape, Earth and Planetary Science Letters, 483, 13–28,		
1274	https://doi.org/10.1016/j.epsl.2017.11.050, 2018.		
12,7	110,000 J 2010 10 J 10 D 10 D		
1275	Liebl, M., Robl, J., Egholm, D. L., Prasicek, G., Stüwe, K., Gradwohl, G., & and Hergarten, S. (2021)		
1276	Topographic signatures of progressive glacial landscape transformation-, Earth Surface Processes and		Formatted: Font: Not Italic
1277	Landforms, 46 (10), 1964–1980-, https://doi.org/10.1002/esp.5139, 2021.		Formatted: Font: Not Italic
1			<u> </u>

1278	Louis, H . (1952): Zur Theorie der Gletschererosion in Tälern-, <u>E&G Quaternary Science Journal</u> , <u>2</u> (1) , <u>1</u>		Formatted: Font: Not Italic
1279	12- <u>-</u> 24-, https://doi.org/10.3285/eg.02.1.02 <u>, 1952.</u>		Formatted: Font: Not Italic
1280	Magnin, F., Josnin, JY., Ravanel, L., Pergaud, J., Pohl, B., ∧ Deline, P. (2017): Modelling rock wall		
1281	permafrost degradation in the Mont Blanc massif from the LIA to the end of the 21st century. The		Formatted: Font: Not Italic
1282	Cryosphere, 11(4), 18131834, https://doi.org/10.5194/tc-11-1813-2017, 2017.		Formatted: Font: Not Italic
			Tornatted. Fort. Not Italic
1283	Malamud, B. D., Turcotte, D. L., Guzzetti, F., & and Reichenbach, P. (2004) Landslide inventories and		
1284 1285	their statistical properties-, Earth Surface Processes and Landforms, 29(6), 687-711-, https://doi.org/10.1002/esp.1064, 2004.	<	Formatted: Font: Not Italic
1283	https://doi.org/10.1002/esp.1004 <u>, 2004.</u>		Formatted: Font: Not Italic
1286	Martin, H. A., Peruzzetto, M., Viroulet, S., Mangeney, A., Lagrée, PY., Popinet, S., Maury, B.,		
1287	Lefebvre-Lepot, A., Maday, Y., ∧ Bouchut, F . (2023) Numerical simulations of granular dam		
1288	break <u>::</u> Comparison between discrete element, Navier-Stokes, and thin-layer models. <u>Physical</u>		
1289	Review, Phys. Rev, E, 108(5), 054902-, https://doi.org/10.1103/PhysRevE.108.054902, 2023.	<	Formatted: Font: Not Italic
1290	Marx, H. E., Dentant, C., Renaud, J., Delunel, R., Tank, D. C., & Lavergne, S. (2017) Riders in the		Formatted: Font: Not Italic
1291	sky (islands):): Using a mega-phylogenetic approach to understand plant species distribution and		
1292	coexistence at the altitudinal limits of angiosperm plant life _{-L} Journal of Biogeography, 44(11),		Formatted: Font: Not Italic
1293	2618–2630-, https://doi.org/10.1111/jbi.13073, 2017.		Formatted: Font: Not Italic
1204	MACCHI C T (2002) - Description and place stability Commonwhaless 452, 454, 4, 40		
1294 1295	McColl, S. T . (2012) Paraglacial rock-slope stability-, Geomorphology, 153—154, 1—16-, https://doi.org/10.1016/j.geomorph.2012.02.015, 2012.	$ \leftarrow $	Formatted: Font: Not Italic
1293	https://doi.org/10.1010/j.geomorpii.2012.02.013 <u>, 2012.</u>		Formatted: Font: Not Italic
1296	Métivier, F., Gaudemer, Y., Tapponnier, P., & and Klein, M. (1999) Mass accumulation rates in Asia	_ `	Formatted: Font: Not Italic
1297	during the CenozoicGeophysical Journal International, 137(2), 280318	1	Formatted: English (United States)
1298	https://doi.org/10.1046/j.1365-246X.1999.00802.x <u>, 1999.</u>		Formatted: English (United States)
1299	Meunier, P., Hovius, N., & And Haines, J. A. (2008) Topographic site effects and the location of		Formatted: English (United States)
1300	earthquake induced landslides-, Earth and Planetary Science Letters, 275(3), 221–232-,	//	Formatted: Font: Not Italic
1301	https://doi.org/10.1016/j.epsl.2008.07.020 <u>, 2008.</u>	$\int_{-\infty}^{\infty}$	Formatted: Font: Not Italic
			Formatted: Font: Not Italic
1302 1303	Micheletti, N., Lambiel, C., & and Lane, S. N. (2015) Investigating decadal-scale geomorphic dynamics in an alpine mountain setting. Journal of Geophysical Research: Earth Surface, 120(10),	1	
1303	Article 10-, 2155–2175, https://doi.org/10.1002/2015JF003656, 2015.	///[Formatted: Font: Not Italic
	74466 10. <u>72133 2173,</u> https://doi.org/10.1001/20133.003030 <u>/2013.</u>		Formatted: English (United States)
1305	Mitchell, S. G., & and Montgomery, D. R. (2006): Influence of a glacial buzzsaw on the height and	///	Formatted: English (United States)
1306	morphology of the Cascade Range in central Washington State, USA-, Quaternary Research, 65(1),	` //	Formatted: English (United States)
1307	96- <u>107</u> - _L https://doi.org/10.1016/j.yqres.2005.08.018 <u>, 2006.</u>		Formatted: Font: Not Italic
1308	Montgomery, D. R., & Korup, O. (2011). Preservation of inner gorges through repeated Alpine		Formatted: Font: Not Italic
1309	glaciations. Nature Geoscience, 4(1), 62-67. https://doi.org/10.1038/ngeo1030	//	Formatted: Font: Not Italic
		,	Formatted: Font: Not Italic
1310	Morriss, M. C., Lehmann, B., Campforts, B., Brencher, G., Rick, B., Anderson, L. S., Handwerger, A. L.,		
1311 1312	Overeem, I., & and Moore, J. (2023) Alpine hillslope failure in the western US: Insights: Insights from the Chaos Canyon landslide, Rocky Mountain National Park, USA., Earth Surface Dynamics,	_	Francis J. Francis Inc. Pr
1312	11(6) , 12511274-, https://doi.org/10.5194/esurf-11-1251-2023, 2023.		Formatted: Font: Not Italic
7	VINE		Formatted: Font: Not Italic
1314	Mudd, S. M., Harel, MA., Hurst, M. D., Grieve, S. W. D., ∧ Marrero, S. M . (2016) The CAIRN		
1315	method : Automated: automated, reproducible calculation of catchment-averaged denudation rates		
1316	from cosmogenic nuclide concentrations- _{1,E} arth Surface Dynamics, 4(3), 655- <u></u> 674-,	<	Formatted: Font: Not Italic
1317	https://doi.org/10.5194/esurf-4-655-2016 <u>, 2016.</u>		Formatted: Font: Not Italic

1318	Müller, T., Lane, S. N., & Schaefli, B. (2022) Towards a hydrogeomorphological understanding of		
1319	proglacial catchments : An: an assessment of groundwater storage and release in an Alpine		
1320	catchment ₋₁ Hydrology and Earth System Sciences, 26 (23) , 6029—6054-,	<u> </u>	Formatted: Font: Not Italic
1321	https://doi.org/10.5194/hess-26-6029-2022 <u>, 2022.</u>		Formatted: Font: Not Italic
1322	Muñoz, E., Ochoa, A., & and Cordão-Neto, M. (2016) Probabilistic assessment of precipitation-		
1323	triggered landslides : The: the role of vegetation . E3S Web of Conferences, Conf., 9, 08001 .		Formatted: Font: Not Italic
1324	https://doi.org/10.1051/e3sconf/20160908001 <u>, 2016.</u>		Formatted: Font: Not Italic
1325	Niemi, N. A., Oskin, M., Burbank, D. W., Heimsath, A. M., and Gabet, E. J.: Effects of bedrock		
1326	landslides on cosmogenically determined erosion rates, Earth and Planetary Science Letters, 237,		
1327	480–498, https://doi.org/10.1016/j.epsl.2005.07.009, 2005.		
1328	Nocquet, JM., Sue, C., Walpersdorf, A., Tran, T., Lenôtre, N., Vernant, P., Cushing, M., Jouanne, F.,		
1329	Masson, F., Baize, S., Chéry, J., ∧ van der-Beek, P. A. (2016): Present-day uplift of the western		
1330	Alps-, Scientific Reports, 6(1), Article 1-, https://doi.org/10.1038/srep28404, 2016.		Formatted: Font: Not Italic
1331	Norton, K. P., Abbühl, L. M., & Schlunegger, F. (2010) Glacial conditioning as an erosional		Formatted: Font: Not Italic
1332	driving force in the Central Alps-, Geology, 38 (7), 655658-, https://doi.org/10.1130/G31102.1,		Formatted: Font: Not Italic
1333	<u>2010.</u>		Formatted: Font: Not Italic
1334	Pedersen, V. K., &. and Egholm, D. L. (2013) Glaciations in response to climate variations		
1335	preconditioned by evolving topography-, Nature, 493 (7431), 206–210-,		Formatted: Font: Not Italic
1336	https://doi.org/10.1038/nature11786 <u>, 2013.</u>		Formatted: Font: Not Italic
1337	Pedersen, V. K., Egholm, D. L., & Nielsen, S. B. (2010) Alpine glacial topography and the rate of		
1338	rock column uplift: A: a global perspective. Geomorphology, 122(1), 129-139.		Formatted: Font: Not Italic
1339	https://doi.org/10.1016/j.geomorph.2010.06.005 <u>, 2010.</u>		Formatted: Font: Not Italic
1340	Peizhen, Z., Molnar, P., ∧ Downs, W. R. (2001): Increased sedimentation rates and grain sizes 2–		
1341	4 Myr ago due to the influence of climate change on erosion rates. Nature, 410(6831), 891-897.		Formatted: Font: Not Italic
1342	https://doi.org/10.1038/35073504 <u>, 2001.</u>		Formatted: Font: Not Italic
1343	Penck, A. (1905) Glacial Features in the Surface of the Alps-, The Journal of Geology, 13(, 1), 1-19-,		Formatted: Font: Not Italic
1344	https://doi.org/10.1086/621202 <u>, 1905.</u>		Formatted: Font: Not Italic
1345	Perron, J. T . (2011) Numerical methods for nonlinear hillslope transport laws, Journal of		Formatted: Font: Not Italic
1346	Geophysical Research: Earth Surface, 116(F2)., https://doi.org/10.1029/2010JF001801, 2011.		Formatted: Font: Not Italic
12.47	Pittish I Bashina A Linhault E Ations C Bina C Good Version Taxis B (2024) Cadimant		Formatted. Forth Not Italic
1347 1348	Pitlick, J., Recking, A., Liebault, F., Misset, C., Piton, G., & and Vazquez-Tarrio, D. (2021) Sediment Production in French Alpine Rivers., Water Resources Research, 57(12), e2021WR030470.	_	Farmattad, Fart, Nat Italia
1349	https://doi.org/10.1029/2021WR030470, 2021.	<	Formatted: Font: Not Italic
7			Formatted: Font: Not Italic
1350	Portenga, E. W., & and Bierman, P. R. (2011) Understanding earth's eroding surface with 10 Be.,		Formatted: English (United States)
1351	College of Arts and Sciences Faculty Publications, https://doi.org/10.1130/G111A.1, 2011.		Formatted: English (United States)
1352	Prasicek, G., Larsen, I. J., and Montgomery, D. R.: Tectonic control on the persistence of glacially	/,	Formatted: English (United States)
1353	sculpted topography, Nat Commun, 6, 8028, https://doi.org/10.1038/ncomms9028, 2015.		Formatted: Font: Not Italic
1354	Prasicek, G., Hergarten, S., Deal, E., Herman, F., ∧ Robl, J . (2020) A glacial buzzsaw effect		
1355	generated by efficient erosion of temperate glaciers in a steady state model-, Earth and Planetary		Formatted: Font: Not Italic
1356	Science Letters, 543, 116350-, https://doi.org/10.1016/j.epsl.2020.116350, 2020.		Formatted: Font: Not Italic
1			

1357 1358	Prasicek, G., Larsen, I. J., & Montgomery, D. R. (2015). Tectonic control on the persistence of glacially sculpted topography. <i>Nature Communications</i> , 6(1), 8028. https://doi.org/10.1038/ncomms9028	
1336	sculpted topography. Nature communications, 9(1), 5026. https://doi.org/10.1036/160hims3026	
1359	Ravanel, L., Magnin, F., & and Deline, P. (2017) Impacts of the 2003 and 2015 summer heatwaves	Formatted: English (United States)
1360	on permafrost-affected rock-walls in the Mont Blanc massif-, Science of The Total Environment, 609,	Formatted: English (United States)
1361	132- <u></u> 143 ₋ _L https://doi.org/10.1016/j.scitotenv.2017.07.055, <u>2017.</u>	Formatted: English (United States)
362	Roering, J. (2012): Landslides limit mountain relief., Nature Geoscience Geosci, 5(7), 446—447.	Formatted: Font: Not Italic
1363	https://doi.org/10.1038/ngeo1511 <u>, 2012.</u>	Formatted: Font: Not Italic
1364	Roering, J. J., Kirchner, J. W., ∧ Dietrich, W. E. (1999): Evidence for nonlinear, diffusive sediment	Formatted: Font: Not Italic
1365	transport on hillslopes and implications for landscape morphology. Water Resources Research,	Formatted: Font: Not Italic
1366	35 (3), 853870-, https://doi.org/10.1029/1998WR900090, 1999.	Formatted: Font: Not Italic
1367	Rootes, C. M., &. and Clark, C. D. (2020) Glacial trimlines to identify former ice margins and	Formatted: Font: Not Italic
1368	subglacial thermal boundaries: A review and classification scheme for trimline expression. Earth-	Formatted: Font: Not Italic
369	Science Reviews, 210, 103355-, https://doi.org/10.1016/j.earscirev.2020.103355, 2020.	Formatted: Font: Not Italic
		Tornacted. Fort. Not Italic
1370 1371	Roussel, E., Marren, P. M., Cossart, E., Toumazet, JP., Chenet, M., Grancher, D., & and Jomelli, V- (2018): Incision and aggradation in proglacial rivers: Post-Little Ice Age long-profile adjustments of	
1371 1372	Southern Iceland outwash plains, Land Degradation & Development, 29(10), 2753-2371.	Formatted: Font: Not Italic
1373	https://doi.org/10.1002/ldr.3127_2018.	Formatted: Font: Not Italic
		Formatted: Font: Not Italic
1374 1375	Scherler, D. (2014) Climatic limits to headwall retreat in the Khumbu Himalaya, eastern Nepal., Geology, 42(11), 1019–1022-, https://doi.org/10.1130/G35975.1, 2014.	Formatted: Font: Not Italic
13/3	Quelogy, 42(11), 1015-1022-, https://www.org/10.1130/033573.1,2014.	Formatted: Font: Not Italic, English (United States)
1376	Schlunegger, F. , & . and Hinderer, M . (2003) Pleistocene/Holocene climate change, re-	Formatted: English (United States)
1377	establishment of fluvial drainage network and increase in relief in the Swiss Alps- ₁₂ Terra Nova, 15(2) ₁₂	Formatted: Font: Not Italic, English (United States)
1378	88- <u>_95</u> -, https://doi.org/10.1046/j.1365-3121.2003.00469.x, <u>2003</u> ,	Formatted: English (United States)
1379	Schwartz, S., Zerathe, S., Jongmans, D., Baillet, L., Carcaillet, J., Audin, L., Dumont, T., Bourlès, D.,	Formatted: English (United States)
1380	Braucher, R., & and Lebrouc, V. (2017) Cosmic ray exposure dating on the large landslide of	Formatted: English (United States)
1381 1382	Séchilienne (Western Alps)-: A synthesis to constrain slope evolution-, Geomorphology, 278, 329- 344-, https://doi.org/10.1016/j.geomorph.2016.11.014, 2017.	Formatted: English (United States)
1302	344- _L nttps://doi.org/10.1010/j.geomorpii.2010.11.014 <u>, 2017.</u>	Formatted: English (United States)
1383	Seguinot, J ., & and Delaney, I . (2021) Last-glacial-cycle glacier erosion potential in the Alps-, Farth	Formatted: English (United States)
1384	Surface Dynamics, 9(4), 923–935, https://doi.org/10.5194/esurf-9-923-2021	Formatted: Font: Not Italic
1385	Shuster, D. L., Ehlers, T. A., Rusmoren, M. E., & Farley, K. A. (2005). Rapid Glacial Erosion at 1.8 Ma	Formatted: Font: Not Italic
1386	Revealed by 4He/3He Thermochronometry. Science, 310(5754), 1668-1670.	Formatted: Font: Not Italic
1387	https://doi.org/10.1126/science.1118519, 2021.	Formatted: Font: Not Italic
 1388	Solomina, O. N., Bradley, R. S., Hodgson, D. A., Ivy-Ochs, S., Jomelli, V., Mackintosh, A. N., Nesje, A.,	Formatted: Font: Not Italic
1389	Owen, L. A., Wanner, H., Wiles, G. C., & and Young, N. E. (2015) Holocene glacier fluctuations	Formatted: Font: Not Italic
1390	Quaternary Science Reviews, 111, 9–34-, https://doi.org/10.1016/j.quascirev.2014.11.018, 2015.	Formatted: Font: Not Italic
1201	Stark C. D. & and Having N. (2001): The characterization of landelide size distributions	/}
1391 1392	Stark, C. P., & and Hovius, N. (2001).: The characterization of landslide size distributions. Geophysical Research Letters, 28(6), 1091—1094., https://doi.org/10.1029/2000GL008527, 2001.	Formatted: Font: Not Italic
	1 - 1 - 1 - 1 - 1 - 1 - 1 - 1 - 1 - 1 -	Formatted: Font: Not Italic, English (United States)
1393	Steer, P., Huismans, R. S., Valla, P. G., Gac, S., & and Herman, F. (2012) Bimodal Plio-Quaternary	Formatted: English (United States)
1394 1395	glacial erosion of fjords and low-relief surfaces in Scandinavia-, Nature Geoscience Geosci, 5(9), Article	Formatted: Font: Not Italic, English (United States)
1292	9-, 635–639, https://doi.org/10.1038/ngeo1549, 2012,	Formatted: English (United States)

Formatted: English (United States)
Formatted: English (United States)

1396	Sternai, P., Herman, F., Valla, P. G., & and Champagnac, JD. (2013) Spatial and temporal variations	Formatted: English (United States)
1397	of glacial erosion in the Rhône valley (Swiss Alps):]: Insights from numerical modeling:, Earth and	Formatted: English (United States)
1398	Planetary Science Letters, 368, 119—131. https://doi.org/10.1016/j.epsl.2013.02.039, 2013.	Formatted: Font: Not Italic
1399	Sternai, P., Sue, C., Husson, L., Serpelloni, E., Becker, T. W., Willett, S. D., Faccenna, C., Di Giulio, A.,	Formatted: Font: Not Italic
1400	Spada, G., Jolivet, L., Valla, P., Petit, C., Nocquet, JM., Walpersdorf, A., & Castelltort, S. (2019)	
1401	Present-day uplift of the European Alps-: Evaluating mechanisms and models of their relative	
1402 1403	contributions-, Earth-Science Reviews, 190, 589-604. https://doi.org/10.1016/j.earscirev.2019.01.005, 2019.	Formatted: Font: Not Italic
1403	https://doi.org/10.1010/j.earschev.2015.01.005 <u>, 2015.</u>	Formatted: Font: Not Italic
1404	Stoffel, M., Trappmann, D. G., Coullie, M. I., Ballesteros Cánovas, J. A., & and Corona, C . (2024). :	
1405	Rockfall from an increasingly unstable mountain slope driven by climate warming. <i>Nature</i>	
1406	Geoscience, Nat. Geosci., 1~_6, https://doi.org/10.1038/s41561-024-01390-9, 2024.	
1407	Tanyaş, H., Allstadt, K. E., & and van-Westen, C. J. (2018) An updated method for estimating	
1408	landslide-event magnitude-, Earth Surface Processes and Landforms, 43(9), 1836-1847.	Formatted: Font: Not Italic
1409	https://doi.org/10.1002/esp.4359 <u>, 2018.</u>	Formatted: Font: Not Italic
1410	Tanyaş, H., van-Westen, C. J., Allstadt, K. E., ∧ Jibson, R. W . (2019) Factors controlling landslide	
1411	frequency-area distributions-, Earth Surface Processes and Landforms, 44(4), 900—917-,	Formatted: Font: Not Italic
1412	https://doi.org/10.1002/esp.4543 <u>, 2019.</u>	Formatted: Font: Not Italic
		Formatted. Form. Not Italic
1413 1414	Tebbens, S. F. (2020). Landslide Scaling : A Review—_Tebbens—_2020—_Earth and Space Science—_Wiley Online Library:	Formatted: Font: Not Italic
1415	https://agupubs.onlinelibrary.wiley.com/doi/full/10.1029/2019EA000662, last access: 21 September	Formatted: Font: Not Italic
1416	2023.	Formatted: Font: Not Italic
		Formatted: Font: Not Italic
1417	Thomson, S. N., Brandon, M. T., Tomkin, J. H., Reiners, P. W., Vásquez, C., ∧ Wilson, N. J. (2010)	Formatted: Font: Not Italic
1418 1419	Glaciation as a destructive and constructive control on mountain building. Nature, 467(7313), 313—317. https://doi.org/10.1038/nature09365, 2010.	Formatted: Font: Not Italic
1713	217. 1 mcps.//won.org/10.1050/mataree5505/2010.	Formatted: Font: Not Italic, English (United States)
1420	Tomkin, J. H ., & and Braun, J. (2002) The influence of alpine glaciation on the relief of tectonically	Formatted: English (United States)
1421	active mountain belts ₋₁ , American Journal of Science, 302 (3), 169—190-	Formatted: Font: Not Italic, English (United States)
1422	https://doi.org/10.2475/ajs.302.3.169 <u>. 2002.</u>	Formatted: English (United States)
1423	Tucker, G. E., & and Hancock, G. R. (2010) Modelling landscape evolution. Farth Surface Processes	Formatted: English (United States)
1424	and Landforms, 35(1), 28–50-, https://doi.org/10.1002/esp.1952, 2010.	
1425	Valla, P. G . (2021) A tribute to Louis (1952) On the theory of glacial erosion in valleys E&G	Formatted: English (United States)
1426	Quaternary Science Journal, 70(2), , 209–212, https://doi.org/10.5194/egqsj-70-209-2021, <u>2021.</u>	Formatted: English (United States)
]	·	Formatted: English (United States)
1427	Valla, P. G., Shuster, D. L., &van der-Beek, P. A. (2011). Significant increase in relief of the European	Formatted: English (United States)
1428 1429	Alps during mid Pleistocene glaciations. Nature Geoscience, 4(10), 688-692. https://doi.org/10.1038/ngeo1242	Formatted: Font: Not Italic
1429	mttps://doi.org/10.1038/nge012/12	Formatted: Font: Not Italic
1430	Valla, P. G., van der Beek, P. A., &., and Lague, D. (2010).∴ Fluvial incision into bedrock :: Insights from	Formatted: Font: Not Italic
1431	morphometric analysis and numerical modeling of gorges incising glacial hanging valleys (Western	Formatted: Font: Not Italic
1432	Alps, France)-1, Journal of Geophysical Research: Earth Surface, 115(F2)-1	Formatted: Font: Not Italic
1433	https://doi.org/10.1029/2008JF001079 <u>, 2010.</u>	Formatted: Font: Not Italic
1434	Van Den Eeckhaut, M., Poesen, J., Govers, G., Verstraeten, G., & Demoulin, A . (2007) :	Formatted: Font: Not Italic
1435	Characteristics of the size distribution of recent and historical landslides in a populated hilly region,	Formatted: Font: Not Italic

1436	Earth and Planetary Science Letters, 256(3), 588–603, https://doi.org/10.1016/j.epsl.2007.01.040		Formatted: Font: Not Italic
1437	<u>2007.</u>	7	Formatted: Font: Not Italic
1438 1439 1440	van der Beek, P., & Bourbon, P. (2008). A quantification of the glacial imprint on relief development in the French western Alps. <i>Geomorphology</i> , <i>97</i> (1), Article 1. https://doi.org/10.1016/j.geomorph.2007.02.038		
1441 1442 1443	von Blanckenburg, F. (2005). The control mechanisms of erosion and weathering at basin scale from cosmogenic nuclides in river sediment. Earth and Planetary Science Letters, 237(3), 462-479. https://doi.org/10.1016/j.epsl.2005.06.030		
1444 1445 1446	Whipple, K. X . (2001) : Fluvial Landscape Response Time: How Plausible Is Steady-State Denudation-??, American Journal of Science, 301(4-5), 313325-, https://doi.org/10.2475/ajs.301.4-5.313, 2001.		Formatted: Font: Not Italic Formatted: Font: Not Italic
1447 1448 1449	Wood, J. L., Harrison, S., ∧ Reinhardt, L. (2015): Landslide inventories for climate impacts research in the European Alps., Geomorphology, 228, 398—408 https://doi.org/10.1016/j.geomorph.2014.09.005, 2015.		Formatted: Font: Not Italic Formatted: Font: Not Italic
1450 1451 1452	Zachos, J., Pagani, M., Sloan, L., Thomas, E., ∧ Billups, K(2001): Trends, Rhythms, and Aberrations in Global Climate 65 Ma to Present-, Science, 292(5517), 686693-, https://doi.org/10.1126/science.1059412, 2001.		Formatted: Font: Not Italic Formatted: Font: Not Italic
1453 1454 1455	Zech, R., Zech, M., Kubik, P. W., Kharki, K., & and Zech, W. (2009) Deglaciation and landscape history around Annapurna, Nepal, based on 10Be surface exposure dating. Quaternary Science Reviews, 28(11), 1106—1118. https://doi.org/10.1016/j.quascirev.2008.11.013, 2009.		Formatted: Font: Not Italic Formatted: Font: Not Italic
1456 1457 1458 1459	Zerathe, S., Lebourg, T., Braucher, R., & Bourlès, D. (2014) Mid-Holocene cluster of large-scale landslides revealed in the Southwestern Alps by 36Cl dating. Insight on an Alpine-scale landslide activity- _L Quaternary Science Reviews, 90, 106-127-L https://doi.org/10.1016/j.quascirev.2014.02.015, 2014.		Formatted: Font: Not Italic Formatted: Font: Not Italic
1460 1461 1462 1463	Zhang, T., Li, D., East, A. E., Walling, D. E., Lane, S., Overeem, I., Beylich, A. A., Koppes, M., ∧ Lu, X. (2022): Warming-driven erosion and sediment transport in cold regions. <i>Nature Reviews</i> , Nat Rev Earth & Environment Environ, 3(12), 832—851. https://doi.org/10.1038/s43017-022-00362-0, 2022.		Formatted: Font: Not Italic Formatted: Font: Not Italic

Page 45: [1] Formatted	Coline Ariagno	02/09/2025 16:31:00
Font: Not Italic		
Page 45: [2] Formatted	Coline Ariagno	02/09/2025 16:31:00
Font: Not Italic	Come Anagno	02/03/2023 10.31.00
Page 45: [3] Formatted	Coline Ariagno	02/09/2025 16:31:00
Font: Not Italic		
Page 45: [4] Formatted	Coline Ariagno	02/09/2025 16:31:00
Font: Not Italic		
Page 45: [5] Formatted	Coline Ariagno	02/09/2025 16:31:00
Font: Not Italic		
Page 45: [6] Formatted	Coline Ariagno	02/09/2025 16:31:00
Font: Not Italic		-
Day 45 171 5	C.P. A.S	02/00/2025 16 21 00
Page 45: [7] Formatted Font: Not Italic	Coline Ariagno	02/09/2025 16:31:00
Tont. Not italic		
Page 45: [8] Formatted	Coline Ariagno	02/09/2025 16:31:00
Font: Not Italic		
Page 45: [9] Formatted	Coline Ariagno	02/09/2025 16:31:00
Font: Not Italic	Comic Anagno	02/03/2023 10.31.00
Page 45: [10] Formatted	Coline Ariagno	02/09/2025 16:31:00
Font: Not Italic		
Page 45: [11] Formatted	Coline Ariagno	02/09/2025 16:31:00
Font: Not Italic		
Page 45: [12] Formatted Font: Not Italic	Coline Ariagno	02/09/2025 16:31:00
Font. Not italic		
Page 45: [13] Formatted	Coline Ariagno	02/09/2025 16:31:00
Font: Not Italic, English (United States)		
Page 45: [14] Formatted	Coline Ariagno	02/09/2025 16:31:00
English (United States)	Comic Ariagno	02,03,2023 10.31.00
Page 45: [15] Formatted	Coline Ariagno	02/09/2025 16:31:00
Font: Not Italic, English (United States)		
Page 45: [16] Formatted	Coline Ariagno	02/09/2025 16:31:00
5		, ,

English (United States)

Page 45: [17] Formatted	Colina Ariagna	02/09/2025 16:31:00
English (United States)	Coline Ariagno	02/09/2023 16:31:00
English (Officed States)		
Page 45: [18] Formatted	Coline Ariagno	02/09/2025 16:31:00
English (United States)	<u> </u>	
Page 45: [19] Formatted	Coline Ariagno	02/09/2025 16:31:00
English (United States)		
Page 45: [20] Formatted	Coline Ariagno	02/09/2025 16:31:00
Font: Not Italic, English (United States)	Comic Anagno	02,03,2023 10.31.00
Tone. Not italie, English (officed states)		
Page 45: [21] Formatted	Coline Ariagno	02/09/2025 16:31:00
English (United States)		
Page 45: [22] Formatted	Coline Ariagno	02/09/2025 16:31:00
Font: Not Italic, English (United States)		
Page 45: [23] Formatted	Coline Ariagno	02/09/2025 16:31:00
English (United States)		5,50,200
,		
Page 45: [24] Formatted	Coline Ariagno	02/09/2025 16:31:00
English (United States)		
Days 45: [25] Farmetted	Calina Arianna	02/00/2025 16-21-00
Page 45: [25] Formatted English (United States)	Coline Ariagno	02/09/2025 16:31:00
Liigiisii (Oilitea States)		
Page 45: [26] Formatted	Coline Ariagno	02/09/2025 16:31:00
English (United States)		
Page 45: [27] Formatted	Coline Ariagno	02/09/2025 16:31:00
Font: Not Italic		
Page 45: [28] Formatted	Coline Ariagno	02/09/2025 16:31:00
English (United States)	Conne / magne	02,03,2020 10.01.00
Page 45: [29] Formatted	Coline Ariagno	02/09/2025 16:31:00
English (United States)		
Page 45: [30] Formatted	Coline Ariagno	02/09/2025 16:31:00
English (United States)		
Page 45: [31] Formatted	Coline Ariagno	02/09/2025 16:31:00
Font: Not Italic		22,00,2020 10.01.00

Page 45: [32] Formatted	Coline Ariagno	02/09/2025 16:31:00
Font: Not Italic		
	· · · · · · · · · · · · · · · · ·	22 (22 (222 44 24 24
Page 45: [33] Formatted	Coline Ariagno	02/09/2025 16:31:00
Font: Not Italic		
Page 45: [34] Formatted	Coline Ariagno	02/09/2025 16:31:00
Font: Not Italic		
Page 45: [35] Formatted	Coline Ariagno	02/09/2025 16:31:00
English (United States)		
Page 45: [36] Formatted	Coline Ariagno	02/09/2025 16:31:00
English (United States)		
Page 45: [37] Formatted	Coline Ariagno	02/09/2025 16:31:00
Font: Not Italic, English (United States)		
Page 45: [38] Formatted	Coline Ariagno	02/09/2025 16:31:00
English (United States)		
Page 45: [39] Formatted	Coline Ariagno	02/09/2025 16:31:00
Font: Not Italic, English (United States)		
Page 45: [40] Formatted	Coline Ariagno	02/09/2025 16:31:00
English (United States)		
Page 45: [41] Formatted	Coline Ariagno	02/09/2025 16:31:00
English (United States)		